Assessing the accuracy of 1-D analytical heat tracing for estimating near-surface sediment thermal diffusivity and water flux under transient conditions

Rau, Gabriel C.; Cuthbert, Mark O.; McCallum, Andrew M.; Halloran, Landon J S; Andersen, Martin S.

Document Version
Peer reviewed version

Link to publication on Research at Birmingham portal

1 **Assessing the accuracy of 1-D analytical heat tracing for estimating near-surface sediment**

2 **thermal diffusivity and water flux under transient conditions**

3 Revised manuscript for resubmission to the *Journal of Geophysical Research (Earth Surface)*

4 Gabriel C. Rau[*,1], Mark O. Cuthbert[1, 2], Andrew M. McCallum[3], Landon J.S. Halloran[1], Martin

5 S. Andersen[1]

6

7 1. Connected Waters Initiative Research Centre, School of Civil and Environmental

8   Engineering, Water Research Laboratory, UNSW Australia, Manly Vale 2093 NSW,

9   Sydney, Australia

10 2. School of Geography, Earth and Environmental Sciences, University of Birmingham,

11   Edgbaston, Birmingham, B15 2TT, UK

12 3. Affiliated with the Connected Waters Initiative Research Centre, UNSW Australia, Manly

13   Vale, Australia

14

15 * Corresponding Author:

16 Gabriel C. Rau (gabriel.rau@unsw.edu.au)

17 UNSW Australia, Water Research Laboratory, 110 King Street, Manly Vale 2093, Australia

18 Phone: +61 2 8071 9850, Fax: +61 2 9949 4188

19

Abstract

Amplitude decay and phase delay of oscillating temperature records measured at two vertical locations in near-surface sediments can be used to infer transient water fluxes, thermal diffusivity and sediment scour/deposition. While methods that rely on the harmonics-based analytical heat transport solution assume a steady-state water flux, many applications have reported transient fluxes, but ignored the possible violation of this assumption in the method. Here, we use natural heat tracing as an example to investigate the extent to which changes in the water flux, and associated temperature signal non-stationarity, can be separated from other influences. We systematically scrutinize the assumption of steady-state flow in analytical heat tracing and test the capabilities of the method to detect the timing and magnitude of flux transients. A numerical model was used to synthesize the temperature response to different step and ramp changes in advective thermal velocity magnitude and direction for both a single-frequency and multi-frequency temperature boundary. Time-variable temperature amplitude and phase information were extracted from the model output with different signal processing methods. We show that a worst-case transient flux induces a temperature non-stationarity, the duration of which is less than 1 cycle for realistic sediment thermal diffusivities between 0.02-0.13 m^2/d. However, common signal processing methods introduce erroneous temporal spreading of advective thermal velocities and significant anomalies in thermal diffusivities or sensor spacing, which is used as an analogue for streambed scour/deposition. The most time-variant spectral filter can introduce errors of up to 57 % in velocity and 33 % in thermal diffusivity values with artifacts spanning ±2 days around the occurrence of rapid changes in flux. Further, our results show that analytical heat tracing is unable to accurately resolve highly time-variant fluxes and thermal diffusivities and does not allow for the inference of scour/depositional processes due to the limitations of signal processing in disentangling flux-related signal non-stationarities from those stemming from other sources. To prevent erroneous interpretations, hydrometric data should always be acquired in combination with temperature records.

1. Introduction

Many measured signals that fluctuate over time exhibit amplitude decay and phase shifting over space caused by time-varying natural processes, for example: seismic wave propagation [Best et al., 1994], depth profiles of soil moisture [Wu et al., 2002], groundwater levels [Cuthbert, 2010] and seafloor temperature depth profiles [Goto et al., 2005]. In water-saturated near-surface aquatic systems natural heat has become a popular tracer to quantify vertical water fluxes [Anderson, 2005; Rau et al., 2014]. This is due to the presence of daily temperature fluctuations on the earth's surface [Stallman, 1965], increasing interest in surface-groundwater exchange fluxes, and developments in measurement technology to miniaturize and automate sensors [Constantz, 2008]. In particular, analytical approaches to invert water fluxes from multi-level temperature records have received much attention and are now common practice. Constantz [2008] correctly predicted that heat tracing will elevate the significance of streambed research to a field of "streambed science".

Few publications in this field of research have sparked as much follow-on research as Suzuki's [1960] and Stallman's [1965] original presentation of the analytical solution to the 1D convective-conductive heat transport equation with a sinusoidal temperature boundary at the top and a constant temperature boundary at infinite depth. Stallman's [1965] model is an extension to the harmonically-forced solution developed by Carslaw and Jaeger [1959], allowing for movement of water by including the first order spatial derivative of temperature. As such, it could be a mathematical description for many physical processes that are gradient driven and adhere to a simplified homogeneous linear second order differential equation.

Stallman's [1965] analytical solution has inspired various method developments and applications. Goto et al. [2005] successfully estimated sediment thermal regimes and the steady-state vertical water flux near a hydrothermal mound at the ocean floor. Hatch et al. [2006] dissected the original analytical solution to estimate time variable fluxes from the amplitude damping and the phase shifting, both contained in the temperature signal over depth. Keery et al. [2007] calculated streambed vertical fluxes using the amplitude damping feature of the temperature-depth record. They extracted the daily sinusoidal component from noisy field records using Dynamic Harmonic Regression (DHR) [Young et al., 1999; Taylor et al., 2007]. McCallum et al. [2012] recombined the two sinusoid features, amplitude and phase, to arrive at two unknowns, streambed thermal diffusivity and advective thermal velocity. Luce et al. [2013] revisited the original differential equation and combined the information contained in amplitude and phase to derive explicit analytical solutions for sensor spacing or streambed thermal

81 diffusivity as well as advective thermal velocity. These papers contain a wealth of methods that
82 can be readily applied to estimate streambed thermal regimes and vertical water fluxes.

83 Further investigated were the impact of parameter uncertainty and non-ideal conditions (such as
84 sediment heterogeneity and a 2D flow field) on the flux results [Lautz, 2010; Shanafield et al.,
85 2011; Roshan et al., 2012; Cuthbert and Mackay, 2013; Irvine et al., 2015]. The increasing
86 popularity of analytical heat tracing methods has led to the development of algorithms that
87 automate the flux quantification from temperature records, namely *Ex-Stream* [Swanson and
88 Cardenas, 2011] and *VFLUX* [Gordon et al., 2012]. These methods are implicitly geared towards
89 quantifying flux time series.

90 What is often overlooked or implicitly assumed in papers that apply methods to quantify fluxes
91 and thermal diffusivities from field temperature records is the fact that the original analytical
92 solution is based on the assumption of steady-state flow. This assumption is in contrast to the
93 aim of understanding natural processes that are commonly transient in nature. While Lautz
94 [2012] experimented in the laboratory with transient fluxes and found that diurnally forced
95 analytical solutions are able to offer sub-daily fluxes in reasonable agreement with the known
96 fluxes of the experiments, McCallum et al. [2012] concluded from field studies that rapid
97 changes in hydraulic forcing (i.e. floods) lead to erroneous fluxes due to violation of the method
98 assumptions. Furthermore, a reversal in the flux direction, as expected during flood events (e.g.
99 the nature of the flood hydrograph as well as return flow of bank storage), complicates the
100 system's thermal response (i.e. memory effect). We suggest that this will lead to potentially
101 flawed flux estimates when quantified using heat tracing methods based on the assumption of
102 harmonic temperature data. This scenario and its implications on heat tracing have not been
103 comprehensively investigated. However, testing the reliability of heat tracing under highly
104 transient flux scenarios is a crucial prerequisite for its further application in advancing process
105 understanding.

106 The aim of this paper is to explore how accurately flux transients can be determined with
107 methods based on harmonic features that are embedded in temperature records (analytical heat
108 tracing). We systematically test a) the streambed thermal response time to flux transients, and b)
109 the accuracy of the water flux, thermal diffusivity and sediment scour/deposition time series
110 inverted with analytical heat tracing. We demonstrate that near-surface sediment has a particular
111 thermal response time to sudden flux transients, i.e. quantifiable time between flux-related
112 thermal disturbance and return to stationarity. Further, we distinguish between the basic thermal
113 response to a harmonic driver and impacts caused by extraction of fixed-frequency harmonic

4

114 components that stem from general non-stationarity and transients in vertical fluxes, including

115 reversals. Finally, we provide guidance under which conditions the quantification of time-

116 variable water flux, thermal diffusivity or sediment scour/deposition from temperature records in

117 combination with diurnally forced analytical solutions are reliable. Our results are generic and

118 could be useful to other areas of geophysics that utilize time-frequency transformation or

119 amplitude and phase extraction of periodically fluctuating signals to quantify natural processes

120 or properties.

121 **2. Methodology**

122 **2.1. Harmonically forced analytical solutions**

123 This investigation is based on the 1D conductive-convective heat transport equation which is

124 discussed in detail in a number of papers [e.g., Suzuki, 1960; Stallman, 1965; Anderson, 2005;

125 Constantz, 2008; Rau et al., 2014] and it will therefore not be stated here again. Rather, we focus

126 on the analytical methods derived from the original solution by Suzuki [1960] and Stallman

127 [1965]. An analytical solution for the propagation of a harmonic temperature signal with depth is

128 given as [Goto et al., 2005]

129 $\quad$ (1) $\quad T(z,t) = \sum_{i=1}^{n} A_i \cdot \exp\left(\frac{v_t z}{2D} - \frac{z}{2D}\sqrt{\frac{\alpha_i + v_t^2}{2}} \right) \cdot \cos\left(\frac{2\pi}{P_i}t - \frac{z}{2D}\sqrt{\frac{\alpha_i - v_t^2}{2}} \right)$

130 where

131 $\quad$ (2) $\quad \alpha_i = \sqrt{v_t^4\left(1+\left(\frac{8\pi D}{P_i v_t^2}\right)^2\right)}.$

132 Here, T is the temperature in the sediment at depth z [L] below the surface, and t [T] is the

133 time. The subscript i represents individual harmonic frequency components with a total of n

134 components. A_i is the temperature amplitude [K], and P_i is the period [T] of the harmonic

135 component i (frequency $f = 1/P$ or angular frequency $\omega = 2\pi/P$). The parameter of interest

136 is the 'advective thermal velocity' v_t [L/T], as it is proportional to the vertical flux (see further

137 below). D [L^2/T] is the effective thermal diffusivity but without the influence of thermal

138 dispersivity as this has been found insignificant for fluxes smaller than ~10 m/d [Rau et al.,

139 2012a]. However, Rau et al. [2012b] reported that D can be underestimated due to additional

140 thermal spread originating from transverse temperature gradients when the solution requires the

141 dimensionality to be reduced to 1-D, even in materials that are considered homogeneous.

142   Equation 1 follows the principle of superposition (Fourier's theorem), which is inherent to the
143   linear heat transport differential equation, and allows isolation of the signal's different sinusoidal
144   components [Goto et al., 2005].

145   The following reviews and summarizes the general approach that is used to quantify vertical
146   fluxes using Equation 1. Options for extracting amplitude and phase of the diel temperature
147   harmonic from noisy temperature time series with different signal processing methods will be
148   discussed later. The advantage of a harmonic signal is that it has two distinct features, amplitude
149   and phase, which allows solving for two unknowns. For a pair of temperature sensors located at
150   different depths (z positive upwards, negative downwards, $z_2 < z_1$) the temperature amplitude
151   ratio A_r and phase shift $\Delta\phi$ (in radians or days) are defined as [Stallman, 1965; Hatch et al.,
152   2006]

153   (3) $A_r = \dfrac{A_2}{A_1}$

154   (4) $\Delta\phi = \phi_2 - \phi_1$

155   Stallman [1965] reported that the sinusoidal temperature signal dampens and shifts phase over
156   depth (Figure 1).

157   Hatch et al. [2006] used both features, amplitude ratio and phase shift, separately to solve for the
158   vertical advective thermal velocity

159   (5) $v_{t,Ar} = \dfrac{2D}{\Delta z}\ln(A_r) + \sqrt{\dfrac{\alpha + v_{t,Ar}^2}{2}}$

160   (6) $v_{t,\Delta\phi} = \sqrt{\alpha - 2\left(\dfrac{4\Delta\phi\pi D}{P\Delta z}\right)^2}$

161   When using Equations 5-6 the disadvantage is that the thermal diffusivity must be known before
162   calculating velocities as it significantly influences the results [Hatch et al., 2010]. Equations 5-6
163   were field tested and results by the two equations were found to differ significantly from each
164   other despite relying on the same thermal parameters [Rau et al., 2010].

165   Luce et al. [2013] revisited Stallman's [1965] original solution and found that amplitude and
166   phase can be combined and expressed as dimensionless velocity as

167   (7) $\eta = -\dfrac{ln(A_r)}{\Delta\phi}.$

168 The combined information in Equation 7 is the ratio between the advective (v_t) and the

169 diffusive (v_d) thermal velocity, as

170 (8) $$v^* = \frac{v_t}{v_d} = \frac{1-\eta^2}{\sqrt{2\eta\left(1+\eta^2\right)}} = \frac{Pe}{2}.$$

171 Conveniently, Pe is the thermal Péclet number indicating dominance of diffusive ($Pe < 1$) or

172 convective conditions ($Pe > 1$). Equation 7 is useful to determine the direction and change of

173 water velocity simply from temperature amplitude and phase information without any further

174 parameters, such as sensor spacing or thermal diffusivity [Luce et al., 2013].

175 The damping depth z_d of the sinusoid is determined as [Goto et al., 2005; Luce et al., 2013]

176 (9) $$z_d = \sqrt{\frac{DP}{\pi}}.$$

177 This is the depth at which the temperature amplitude is damped to $1/e$ of its original value.

178 Assuming a constant sensor spacing (Δz), the thermal diffusivity can be calculated using [Luce

179 et al., 2013]

180 (10) $$D = \frac{2\pi\eta\Delta z^2}{P\left(ln^2\left(A_r\right)+\Delta z^2\right)}$$

181 It is noteworthy that results from this equation are equivalent to that published by McCallum et

182 al. [2012]. They reported that the thermal diffusivity calculated using field data can exceed

183 physically possible values during periods when the stream stage rapidly changes (transient flux

184 conditions). While they suggested that the method may break down during such conditions, they

185 did not investigate its limitations in correctly resolving parameters over the duration of transient

186 conditions.

187 Analogously, assuming a constant thermal diffusivity (D), the sensor spacing (Δz) is

188 determined as [Luce et al., 2013; Tonina et al., 2014]

189 (11) $$\Delta z = z_d\sqrt{\frac{ln^2\left(A_r\right)+\Delta\phi^2}{2\eta}}$$

190 Interestingly, Luce et al. [2013] and Tonina et al. [2014] have used this to quantify sediment

191 scour/depositional processes, indicated by a time variable sensor spacing, based on field data

192 obtained during a period of transient stream discharge. However, they did not consider the

193   possible limitations that transient fluxes can impose on methods based on the diurnal heat
194   forcing. Here, it is important to note that equations 10 and 11 are exactly the same and can either
195   quantify sediment thermal diffusivity (D) or scour/depositional processes inferred from sensor
196   spacing (Δz).

197   Finally, the advective thermal velocity is determined using [Luce et al., 2013]

198   (12)
$$v_t = \frac{2\pi\Delta z\left(1-\eta^2\right)}{P\sqrt{\left(1+\eta^2\right)\left(ln^2\left(A_r\right)+\Delta z^2\right)}}.$$

199   Equation 13 is the final step to quantify the Darcy flux (q) from advective thermal velocity as

200   (13)
$$q = \left(\varepsilon+\left(1-\varepsilon\right)\frac{c_s^v}{c_w^v}\right)v_t$$

201   where additional sediment properties are required: ε is the porosity of the sediment, c_s^v and c_w^v
202   are the volumetric heat capacities of the solids and water, respectively. Equation 13 is stated here
203   for sake of completeness, but will not be used further to quantify the Darcy flux, since this is not
204   the aim of the paper. Instead, we let the advective thermal velocity, v_t, represent the convective
205   conditions (vertical flux magnitude and direction). In this paper we use Equations 3-12 to invert
206   fluxes from temperature data that has been generated by a numerical model described in the next
207   section.

208   **2.2. Numerical modeling**

209   In this paper a transient numerical model was used to generate the thermal response $T\left(z,t\right)$ to
210   step and ramp changes in the water velocity (i.e. worst case transient scenario). The conceptual
211   model is a diurnally forced water saturated near-surface system (i.e. like a streambed). The
212   approach is an analogue to any real-world transient flux signal, as this can be thought of as
213   multiple discrete-time steps with variable magnitudes and durations.

214   COMSOL Multiphysics V5 [COMSOL, 2014] was used as the numerical solver for the
215   conductive-convective heat transport equation in a one-dimensional domain, resembling the
216   vertical extent of a near-surface hydrologic system. For all simulations a sinusoidal temperature
217   signal with period $P=1$ day and amplitude of 3 °C at a mean of 20 °C was applied at the top of
218   the domain. The bottom of the domain was held at a constant temperature of 20 °C at a large
219   enough distance (30 m) to have no further effect on the simulated temperatures in the upper 1 m

220   used in the analysis. The initial condition was T = 20 ºC across the whole model domain. The

221   mesh increased in size from 4 mm at the upper boundary to 1 cm at the base of the domain. The

222   absolute solver tolerance was set to $1 \cdot 10^{-5}$ ºC with a relative tolerance of $1 \cdot 10^{-9}$, small enough

223   to ensure that the model output was no longer sensitive to changes in these values. The

224   numerical models were accurate to within ~0.0001 °C against the range of analytical models

225   during steady velocity periods.

226   Each simulation was conducted for a total time of 30 days with a constant advective thermal

227   velocity assigned to the first 10 days, followed by a step change in advective thermal velocity

228   and another 20 days of simulation. Temperature records were generated at 96 time steps per day

229   (15 min time step) at the top boundary and at the depths: 0.02 m, 0.05 m, 0.1 m, 0.2 m, 0.3 m,

230   0.5 m, 0.75 m and 1 m (see dashed horizontal lines in Figure 1). The large number of depths

231   allowed investigation of both up- and downward flow by evaluating data from sensor locations

232   at depths where the temperature signal was not damped beyond recognition (temperature

233   variations well above the limits of typical field instrument resolution, typically 0.001-0.01 ºC).

234   The following transient advective thermal velocity scenarios were simulated in separate sub

235   cases:

236   1.   0 m/d followed by a downward step change: -0.01, -0.1, -0.5, -1 and -5 m/d,

237   2.   0 m/d followed by an upward step change: 0.01, 0.1, 0.5, 1 and 2 m/d,

238   3.   Reversal step change from -1 m/d downwards to 1 m/d upwards, and from 1 m/d

239   upwards to -1 m/d downwards,

240   4.   Linear increase from 0 to -1 m/d within a time of 0.5, 1, 2 and 4 days.

241   The velocity reversals are particularly interesting as the thermal signal is transported downwards

242   and then upwards (or vice versa) by the water flux by convection while conducting

243   simultaneously depending on the temperature-depth gradient. The linear streambed velocity

244   increases represent the likely responses to different hydrograph characteristics, for example fast

245   flux transient caused by flash flooding, or slow flux transients due to snow melt.

246   To illustrate the influence of the thermal diffusivity on the results, all cases were simulated for

247   physically realistic minimum and a maximum thermal diffusivity as reported in the literature

248   [i.e., Shanafield et al., 2011; McCallum et al, 2012]. The numerically simulated temperature time

249   series were first processed using different signal extraction methods, and then Equations 3-12

250   were used to invert for time series of transient velocities and thermal diffusivities. To provide

251   quantifiable measures of the suitability of heat tracing during transient velocities we calculate

9

252 the maximum error and the root-mean-square error (RMSE) between the modeled and inverted

253 advective thermal velocity and diffusivity data. Finally, we test how well signal processing

254 techniques can distinguish between temperature signal non-stationarity caused by flux transients

255 and other processes by repeating the first set of model simulations with a previously measured

256 and published temperature record [Rau et al., 2010] as the upper boundary.

2.3. Extraction of harmonic amplitudes and phases from temperature records

258 A prerequisite to the calculation of water flux and thermal diffusivity are temperature time series

259 measured by sensors in at least two different depths of the water-saturated sediment. From these

260 measurements the strongest frequency component, the daily frequency [Stallman, 1965; Hatch et

261 al., 2006; Keery et al., 2007], is commonly extracted. Here, we evaluate the capability and

262 accuracy of the four most commonly used signal processing techniques that offer time-

263 dependent amplitude and phase extraction. To obtain amplitude and phase data from the

264 sinusoidal component embedded in typically noisy field data a transformation of data from the

265 time domain into the frequency domain is needed.

2.3.1. Harmonic peak identification

267 As a benchmark for the results obtained from different signal processing methods the peak

268 amplitudes and timings were directly identified from the model output. This is only appropriate

269 when the signal consists of a single harmonic frequency as was required by Equations 3-12 and

270 as used for the numerical model. The sampling frequency will limit how accurately peaks

271 (minima and maxima) can be determined. This means that amplitudes and phases may not be

272 optimally detected as any particular minima or maxima may not occur exactly at the sampling

273 time. We apply an algorithm that uses the neighboring values around the peaks to find the exact

274 magnitude and timing with 2nd order polynomial regression. This approach results in a best

275 possible peak time-resolution offering 2 samples per day for peaks. We refer to this approach as

276 "peak picking".

2.3.2. Windowed Fourier Transform (WFT)

278 The most obvious method is the discrete Fourier transform (DFT) and its computational

279 representation, the fast Fourier transform (FFT). A common approach to obtain frequency

280 information is to apply the FFT to a fixed time window that is shifted along the complete record

281 resulting in the windowed Fourier transform (WFT). This approach was suggested by Keery and

282 Binley [2007] and successfully used by Cuthbert et al. [2011].

283 WFT offers the advantage of being able to identify signal non-stationarity, as a measure of

284 transient fluxes, in the time domain. However, it is well known that the WFT has a constant

285 frequency resolution due to the fact that the window size used in the time domain defines the

286 resolution in the frequency domain [Oppenheim and Schafer, 1989]. This means that the window

287 size must have an appropriate amount of samples so that the frequency resolution can capture

288 information at 1 cpd. This amounts to window sizes that are multiples of samples per day (one

289 cycle based on daily fluctuations). Further, the minimum window size must be one harmonic

290 cycle in the time domain as otherwise the discrete samples in the frequency domain do not

291 coincide with the desired frequency. While increasing the window size will reduce the artifacts

292 from spectral leakage, this will also diminish the ability to accurately detect the exact timing of

293 changes in the water flux. Since the focus is on determining transient fluxes the minimum

294 window size, a 1 day window with 96 samples (for our sampling interval of 15 min), was used.

295 To maximize the frequency-time information the window was continuously shifted by 1 sample

296 at a time. This approach is equivalent to a moving rectangular window. While different window

297 shapes will change the extracted amplitude-phase relationship, we focus on avoiding any side

298 effects arising from window functions. The amplitude and phase information, given as the length

299 and angle of the complex FFT output, were assigned to the midpoint of the time window.

300 Amplitudes and phases were then used to quantify fluxes and thermal diffusivities with

301 Equations 3-6, 10 and 12.

2.3.3. Zero-phase (forward-backward) filtering

303 A slightly different amplitude and frequency extraction technique was suggested by Hatch et al.

304 [2006]. Their attempt of recovering the full daily harmonic component in the time domain

305 deployed a windowed filter. The first step is similar to that previously explained for WFT, but

306 then the frequency spectrum is multiplied with a band-pass window centered on 1 cpd to retain

307 the daily frequency and cancel the lower and higher components. This is equivalent to a time-

308 domain convolution of the signal and filter kernel but is often computationally easier. This 1 cpd

309 frequency record is subsequently inverted back to the time domain. Here, the choice of window

310 will have an effect on the spectral leakage, and the *Tukey* window was suggested because it

311 provides an optimization between maintaining the gain for the desired frequency and optimizing

312 the fade of side-band components [Harris, 1978]. The window size (filter order) must be

313 multiples of days to allow accurate sampling of the 1 cpd frequency. Since manipulating the

314 amplitude information in the frequency domain will inevitably also modify the phase

315 information, a forward-backward filter (e.g., Matlab's *filtfilt* function implemented in the Signal

316 Processing Toolbox) must be deployed to allow an exact cancelation of the phase error
317 introduced when filtering in the forward direction only [Hatch et al., 2006].

318 Again, while an increasing window size will result in increasing filter stability it also reduces the
319 temporal resolution (i.e. makes it harder to accurately identify flux transients). A minimum filter
320 order of 384 (= 4 days at 15 min sampling intervals) was determined to result in a stable time-
321 domain output. The filter output in the time domain must undergo "peak picking" before fluxes
322 can be calculated [Hatch et al., 2006].

2.3.4. Continuous Wavelet Transform (CWT)

324 One significant limitation of the Fourier transform is the Heisenberg–Gabor limit, the
325 relationship between resolution in frequency and time domain [Havin and Jöricke, 1994].
326 However, time-varying amplitude and phase information, as measured for time-varying flux and
327 thermal diffusivity, implies that the signal is non-stationary. The continuous wavelet transform
328 (CWT) appears to be better suited for extracting time-variant frequency domain features from
329 temperature records. Onderka et al. [2013] successfully tested the application of CWT in
330 analytical heat tracing. Pidlisecky and Knight [2011] use CWT to derive infiltration rates from
331 1-D resistivity records. For a useful practical guide to the CWT the interested reader is referred
332 to Torrence and Compo [1998]. Further, Grinsted et al. [2004] offer an excellent practical
333 overview of the wavelet transforms and its application to geophysical time–series.

334 Here, we adopt the same approach as was deployed by Onderka et al. [2013] using the *Morlet*
335 mother wavelet because of its close alignment with the harmonic waveform. In the time domain
336 this wavelet is a superposition of a harmonic and the Gauss function with maximum weight
337 given to the center of the window in the time domain. The wavelet can be stretched or
338 compressed depending on the desired frequency to be analyzed. We used the CWT implemented
339 in Matlab by Erickson [2014].

2.3.5. Dynamic Harmonic Regression (DHR)

341 Keery et al. [2007] used Dynamic Harmonic Regression (DHR) to extract the diel harmonic
342 from discrete-time temperature records measured at multiple depths in the sediment. DHR was
343 developed by Young et al. [1999] as an extension to Fourier analysis that is particularly suitable
344 for non-stationary signals. The technique is a data based mechanistic approach that features
345 time-variable spectral coefficients that estimate signal amplitude and phase information [Vogt et
346 al., 2010]. DHR is readily implemented in Matlab as the CAPTAIN toolbox [Taylor et al., 2007]
347 and is a state-of-art choice of filter for a non-stationary signal [Young et al., 1999]. For best

348 compatibility with recent research we implemented DHR in the same way as Keery et al. [2007],

349 Vogt et al. [2010] and in VFLUX [Gordon et al., 2012]. The reader is therefore referred to these

350 papers for further details. Noteworthy is the recommendation for an optimum sampling

351 frequency of 12 samples per day, as over- and under-sampling can cause incorrect signal

352 identification by the DHR algorithm [Gordon et al., 2012].

353　**3. Results and discussion**

354　**3.1. Properties of field temperature records and the harmonically-forced analytical**

355　　　　**solution**

356　As a first point it is vital to consider the characteristics of temperature signals measured in

357　sediments. It is apparent from a number of existing studies that the temperature signal is

358　dominated by the diel and, if the record is long enough, annual frequency [i.e., Hatch et al.,

359　2006; Keery et al., 2007; Wörman et al., 2012]. However, the record typically contains other

360　frequency components that are often referred to as noise. The annual and diel components are

361　controlled by the continuous celestial movements, and thus can be considered harmonics with

362　precisely known cycles (e.g., $P_{diel} = 86,400$ s). More complicated to determine are the "noisy"

363　components which will depend on various natural factors, for example the local climate, site and

364　seasonal specific details (i.e. shading) and sensor noise.

365　The Fourier Theorem stipulates that a continuous function can be decomposed into an infinite

366　series of individual harmonics with different amplitudes and phases. In practice, temperature

367　measurements are recorded digitally as discrete samples in time. Therefore, the signal can be

368　decomposed into a finite series of harmonics using the Discrete Fourier Transform (DFT).

369　However, it is important to consider that each of the components identified by the DFT is a

370　stationary harmonic, and that the resolution in the time domain will also determine the frequency

371　domain resolution [Oppenheim and Schafer, 1989].

372　Also noteworthy here is the fact that the differential heat transport equation is of linear nature.

373　This means that the sediment depth response to any temperature signal at the surface is the sum

374　of the individual harmonics that form part of the original signal, but each weighted according to

375　Equation 1 [Goto et al., 2005]. Importantly, the weighting depends on the signal frequency (

376　$f = 1/P$, note P_i in Equation 1) and the water flux, which translates into exponentially damped

377　amplitudes and linearly shifted phases (Figure 1). In other words, the water flux modulates the

378　depth propagation of harmonics. Quantifying the vertical flux from the properties of individual

379　harmonics, i.e. using the amplitude damping and phase shifting, is exactly what heat tracing

380　methods intend to achieve. In essence, the sediment acts as a frequency filter where faster

381　frequencies are damped quicker and slower frequencies propagate further as a function of the

382　vertical flux [Hatch et al., 2006]. This phenomenon has been exploited to calculate thermal

383　diffusivity and a steady-state vertical flux from temperature spectra [Wörman et al., 2012]. It is

384　clear that diel amplitudes and phases cannot simply be selected from unfiltered temperature

385   records, as has been previously done [Fanelli and Lautz, 2008; Lautz, 2010], because the "noise"

386   which consists of inherently different frequencies distorts the diel signal in a depth and flux

387   dependent way. Extraction of amplitude and phase information with signal processing

388   techniques is therefore a crucial component of heat tracing with diurnally forced analytical

389   solutions.

390   In the context of heat tracing it is important to remember that stationary signals require that their

391   statistical properties – here, the features describing a sinusoidal wave – do not change over time

392   [Oppenheim and Schafer, 1989]. When this is considered in relation to Equation 1, it becomes

393   clear that when a hypothetically stationary temperature harmonic (i.e., a temperature sinusoid at

394   the upper boundary) propagates over depth its stationarity is maintained only if the vertical water

395   flux is in steady-state ($v_t = const$ in Equation 1). Importantly, any transients in the water flux

396   (advective thermal velocity $v_t = f(t)$ in Equation 1) will transform a previously stationary

397   harmonic into a non-stationary signal. Figure 2 illustrates this point using a step change in the

398   water flux as a worst case transient for a pure harmonic (a) and actual temperature (b) data

399   obtained from Rau et al. [2010]. In essence, any flux transient, equivalent to a time-change in the

400   advective thermal velocity (v_t) in Equation 1, will influence the stationarity of the temperature-

401   time signal (see also Figure 1) and thus add to any existing non-stationary features already

402   embedded in the temperature signal (Figure 2b).

403   In reality many field studies that develop and apply analytical heat tracing to gain

404   hydrogeological process understanding are interested in the changes in water flux over time. In

405   other words, they rely on the fact that the analytical heat tracing can detect flux transients [e.g.,

406   Hatch et al., 2006; Keery et al., 2007; Lautz et al., 2010; Rau et al., 2010; Swanson and

407   Cardenas, 2010; Vogt et al., 2010; Jensen and Engesgaard, 2011; Munz et al., 2011; McCallum

408   et al., 2012; Luce et al., 2013; McCallum et al., 2014; Tonina et al., 2014; Gariglio et al., 2014].

409   Here, we test whether flux transients can be quantified using analytical methods and determine

410   their behavior when the temperature signal becomes non-stationary caused by transient fluxes.

411   From a signal processing perspective it is useful to investigate how accurately the onset of

412   sudden signal non-stationarity can be delineated and attributed to a cause, such as changes in the

413   water flux implicitly expressed in the temperature records.

3.2. System response to sudden water flux transients

It is important to understand the thermal modulation of transient fluxes before proceeding with the analysis of signal amplitude and phase extraction methods, and their subsequent impact on the quantification of thermal diffusivities or sediment scour/deposition and the temporal fluxes. This provides the foundation for a quantitative assessment of the possible artifacts that signal processing imposes on the physical processes contained within temperature harmonics.

How long does it take for a harmonic temperature signal to return to stationarity when affected by a sudden change in flux, e.g. a step change? Figure 3a shows the sediment thermal response to sudden advective thermal velocity transients. This is defined as the difference between the numerically modeled temperature response to a velocity step change and the stationary temperature signals that were calculated with Equations 1-2 for the two different steady-state velocities that the step consists of. The thermal response is shown for two different depths and a minimum, average and maximum thermal diffusivity (as was used by Shanafield et al. [2011] and McCallum et al. [2012]). After an initial temperature jump (sharp non-stationarity) caused by the velocity step it is clear that the underlying thermal response resembles the characteristic exponential relaxation described by the generic equation $\exp(-t/\tau)$, where τ is the response time [T]. The magnitude of the temperature non-stationarity induced by the velocity step decreases from approx. 2.3 °C to 0.2 °C (for a boundary amplitude of 3 °C) with increasing thermal diffusivity (Figure 3a). The relaxation time τ for $D_{avg} = 0.075$ m^2/d is approx. 0.15 days, but this depends on the speed of propagation (velocity magnitude and depth of measurement) and the sediment thermal diffusivity. Figure 3a reveals that the minimum thermal diffusivity causes the largest initial temperature jump but also the shortest thermal response time (~0.04 days for a spacing of 0.1 m).

Not surprisingly, the sediment thermal response will also depend on the timing of the velocity transient in relation to the phase of the upper harmonic temperature boundary. Figure 3b shows an example of the velocity step change with the onset occurring at 8 different times shifted by 0.125 days ($\pi/4$ for $f = 1$ cpd). Again, the sediment thermal response at depth was calculated as the difference between the temperature output from the numerical model and the analytical solution. Interestingly, the magnitude of the thermal response ranges between ~0.1 °C and 1.4 °C for the step at 0.125 d and 0.375 d, respectively, and with shape of the sediment thermal response suggesting a more complex function compared to just an exponential relaxation. Nevertheless, the perturbation decays over time as expected.

446   In summary, a water flux step change causes a sudden propagation of non-stationarity in the

447   temperature signal over depth followed by gradual return to stationarity over time. This is due to

448   the previously stationary temperature-depth harmonic being moved downwards or upwards by

449   the sudden change in water flux before stationarity is reached again. For the velocity used in this

450   example and for realistic thermal diffusivities ($0.02 < D < 0.13$ m^2/d) the sediment response

451   time is $0.04 < \tau < 0.24$ days. Importantly, it is evident that the temperature non-stationarity

452   caused by a worst-case transient velocity (step change) diminishes within one harmonic cycle (1

453   day).

454   **3.3. How do different signal extraction methods perform when the signal is non-**

455   **stationary?**

456   Figure 2b suggests that the temperature non-stationarity caused by a transient water flux is

457   superimposed on temperature signal non-stationarities caused by other factors (see earlier

458   discussion). While the importance of correctly extracting amplitudes and phases was established

459   earlier, it is vital to reveal how different signal extraction techniques respond to non-stationarity

460   caused by only the transient water flux, since these transients are of main interest. Hatch et al.

461   [2006] discussed the possible impact of signal filter edge effects on the fluxes and suggested that

462   the effect of filtering should be further investigated. While different authors have used various

463   different signal processing techniques [Hatch et al., 2006; Keery et al., 2007; Cuthbert et al.,

464   2011; Onderka et al., 2013], their impact on the flux results have mostly been assumed

465   negligible, and were neither comprehensively investigated nor quantified.

466   Here, we raise the question: How accurate are different signal processing techniques in

467   delineating non-stationary harmonic features (e.g. amplitudes and phases) caused by transient

468   fluxes when they are buried in a "noisy" signal? This can be answered by comparing the

469   response of signal extraction techniques to a sudden non-stationarity. Figure 4 illustrates the

470   response of four different signal processing techniques (WFT, filtfilt, CWT and DHR; see

471   methods section for details) to the non-stationarity of an otherwise harmonic temperature signal

472   caused by a step change in advective thermal velocity. Figures 4a, 4c, 4e, 4g show the extracted

473   amplitudes and 4b, 4d, 4f, 4h the phases at different depths with time relative to the non-

474   stationarity. Since both amplitude and phase are combined to invert the vertical velocity and

475   thermal diffusivity (see Equations 7-12) it is essential to inspect both separately.

476   Figure 4 demonstrates the following features:

477   ▪   The four signal processing techniques demonstrate different responses to non-stationarity

17

- While the extracted signal amplitudes are generally smooth, the phase data can exhibit significant artifacts, e.g. oscillations (Figure 4b,d,f,h)
- The response to signal non-stationarity is an erroneous temporal spreading ("smearing") over time, with both the amplitude and phase responding before the actual velocity transient has occurred
- Significant "smearing" occurs for a minimum of 1 cycle for WFT (Figure 4a,b), and maximum time of ~3 cycles for filtfilt (Figure 4c,d)
- The WFT methods shows strong oscillations in particular for phase data where the signal to noise ratio is low, e.g. for the deepest observation points (Figure 4b)

In general, the above observations highlight that signal processing can strongly impact the quantification of vertical fluxes and thermal diffusivities during transient changes.

3.4. Quantification of transient fluxes and thermal diffusivities

The previously presented amplitude and phase data (Figure 4) were used to derive amplitude ratios (Equation 3) and phase shifts (Equation 4) based on two observation points located at different depths. Then, the velocities and thermal diffusivities were quantified from Equations 7-12 and compared with those used as input to the numerical model. This was done with amplitude and phase data extracted using all four signal processing techniques (Figure 4). Figure 5 summarizes the vertical velocities (a, c, e, g) and thermal diffusivities (b, d, f, h) for different velocity step changes, 0 to -1 m/d (a & b), 0 to 1 m/d (c & d), reversal from -1 m/d to 1 m/d (e & f) and reversal from 1 m/d to -1 m/d (g & h). As a best-case benchmark the results from picking amplitudes and phases straight from the simulated temperature data (which is possible in this case since a sinusoidal temperature boundary is used), are also shown. We emphasize that this approach presents the best possible time resolution that can be achieved from methods that rely on a harmonic signal, as a sinusoid only has 2 features per cycle (amplitudes and phases at maximum and minimum).

Figure 5 shows significant artifacts in vertical velocities and thermal diffusivities that stem from quantifying the heat tracing derived velocity over a step change in the modeled water velocity. Best results are achieved when peak picking is applied to unfiltered harmonic temperature data (red squares in Figure 5) showing only a small deviation from the modeled velocity. The errors between modeled and inverted velocity are caused by the streambed's non-stationary thermal response, as was discussed earlier (Section 3.2, Figure 3). However, this approach can only be

509 used when the temperature signal is a pure harmonic (stationary) and must not be applied to

510 noisy real-field measurements.

511 Being deduced from the previously shown amplitude and phase data (Figure 4) the velocity and

512 diffusivity results are also "smeared" across ~4-5 cycles, approximately centered at the time at

513 which the transient velocity occurred (Figure 5). It is noteworthy that for downward velocity

514 steps the thermal diffusivity is overestimated, and it is underestimated for upward velocity steps.

515 Note that sensor spacing (Equation 11) is prone to the same anomaly because it originates from

516 reformulating the thermal diffusivity (Equation 10). Figures 6 and 7 show the same calculation

517 for different velocity step sizes in both directions and found that the response becomes

518 increasingly smeared and delayed for large velocity steps. Interestingly, the results in Figures 5,

519 6 and 7 also indicate that for velocity steps up to ±1 m/d the "smearing" is independent of either

520 the velocity step magnitude or direction, even for velocity reversals. Further, results show that

521 for velocity transients exceeding -5 m/d (Figure 6) and 2 m/d (Figure 7) the response shifts

522 forward in time and the error between modeled and inverted advective velocity increases

523 significantly.

524 These results demonstrate that signal processing techniques, and not the assumption of steady-

525 state flux inherent to the analytical solution (Equation 1), is the culprit responsible for inaccurate

526 detection of transient fluxes quantified from harmonically forced analytical solutions. This is due

527 to the uncertainty principle (Heisenberg-Gabor limit) based on fixed resolution in both time and

528 frequency domain inherent to any signal filtering that relies on the Fourier transform [Havin and

529 Jöricke, 1994].

530 While the scenarios presented in Figures 5-7 resemble a worst case caused by highly transient

531 hydrographs (e.g. flash floods, dam releases), streams that are dominated by snowmelt typically

532 experience slower flux transients. Figure 8 shows the response of heat tracing to different rates

533 of velocity change (an analogue of the hydrograph slope assuming no change of hydraulic

534 conductivity over time) modeled as a linear increase of the advective thermal velocity from 0 to -

535 1 m/d within 0.5, 1, 2 and 4 days. A summary of the match between modeled and inverted

536 advective thermal velocities and diffusivities can be found in Tables 1 and 2, respectively, for

537 the four different filtering methods and the four different rates of velocity change (Figure 8) as

538 well as the step change (first row in Figure 5). Here, it is interesting to note that the velocities

539 inverted without applying any signal processing methods directly from the temperature

540 amplitudes and phases (red markers) in all cases closely resemble the actual velocities used to

541 drive the numerical model (Figure 8 first column, RMSE < 0.031 ºC in all cases). In contrast

542   inverted thermal diffusivities (or sensor spacing) are more sensitive to flux transients, with

543   values generally underestimated and with decreasing errors for a decreasing rate of velocity

544   change (Figure 8 second column). The time decay of the error is in agreement with the

545   streambed thermal response evaluated in Figure 3.

546   Figure 8 further illustrates the capability of the different signal processing methods to delineate

547   different degrees of signal non-stationarity. As expected, the less transient the better the response

548   of signal processing methods, indicated by the degree of matching between modeled and

549   inverted velocity (decreasing RMSE in Table 1). It is apparent that DHR is the overall best

550   performing (most time-variant) method with inverted and modeled velocities matching the

551   closest (smallest RMSE in Tables 1 and 2). By contrast, CWT shows the slowest response to

552   velocity transients (highest RMSE in Tables 1 and 2). Interestingly, thermal diffusivities inverted

553   after applying the signal processing methods are consistently overestimated during the velocity

554   transient. Further, it is noteworthy that there remains a significant error in the inverted velocities

555   (max. 0.06 m/d for DHR) and diffusivities for a velocity ramp that spans 4 harmonic cycles. This

556   proves that heat tracing results are increasingly affected by the signal processing methods under

557   increasing transient advective velocities (see RMSE values in Tables 1 and 2). Sudden flux

558   transient can cause errors of up to 57 % in velocity (Table 1) and 37 % in thermal diffusivity

559   (Table 2) estimates even when DHR, the most time-variant spectral filter, is used. Inaccuracies

560   in the inverted results persist for up to ±2 days around the occurrence of sudden flux transients

561   (Figures 5 and 8). The mildest case of velocity transient studied here (-1 m/d velocity change in

562   4 days: $dv/dt = 0.25$ m/d^2) introduces an error of ~6 % in velocity (Table 1) and ~4 % in

563   thermal diffusivity (Table 2) with inaccuracies during ±1 days of the start and end of the velocity

564   change (Figures 8 and first row in Figure 5). These errors are larger for all other signal

565   processing methods and rates of velocity change studied.

566   McCallum et al. [2012] have reported spurious thermal diffusivities in their field investigation

567   during highly transient flow conditions, e.g. dam releases and floods. Further, they found that

568   water flux calculated by heat tracing reacted before the change in hydraulic gradients. Both

569   observations are consistent with the erroneous delineation of transient fluxes caused by signal

570   processing as illustrated in this paper (see Figures 5 and 6). It has previously been suggested that

571   sub-cycle resolution for vertical fluxes can be obtained [Lautz, 2012]. Here, we demonstrate

572   that, while signal processing techniques offer sub-cycle resolution values for amplitudes and

573   phases, the smoothing of the inverted fluxes across sudden transients (and oscillations in the case

574   of phase data) may not resemble the actual transient flux. It is therefore not recommended to

575 trust flux and thermal diffusivity or sediment scour/deposition results during times when fluxes

576 are expected to be transient (e.g. floods). This suggests that hydraulic head data should be

577 interpreted together with temperature data in order to assess transient conditions; otherwise the

578 use of heat tracing based on harmonic signals becomes untrustworthy.

579 The above discussion raises the question as to which signal processing technique performs best

580 under transient flux conditions. Figure 5 suggests that there is no simple answer, as there appears

581 to be a trade-off between the distortion of the magnitude and the duration of the flux and

582 diffusivity estimates. The most suitable approach will depend on the individual circumstances

583 and whether the focus lies on estimating the magnitude or timing of transient fluxes.

584 **3.5. Biased process estimates caused by a non-stationary temperature boundary**

585 While the previous discussion revealed that signal processing techniques hamper the accurate

586 time-resolution of quantified fluxes and thermal diffusivities or sediment scour/deposition when

587 the water flux is transient, the influence of non-stationarity in the field temperature records has

588 so far been neglected but must also be considered. Rau et al. [2010] measured the temperatures

589 at the bottom of the stream column and at several depths within the streambed sediment with a

590 sensor spacing of 0.15 m at 3 different horizontal locations within a small perennial stream in

591 Australia over a 3-month period in 2007. Here, we use a 30-day subset of the uppermost

592 temperature data from location C (see Rau et al. [2010]) as a real-field boundary condition for

593 our numerical model. Figure 9a shows the multi-level temperature time series obtained from

594 numerical modeling using a velocity step change and the measured surface water temperature as

595 the boundary condition [Rau et al. 2010]. Here, the non-stationarity is present in the system due

596 to both natural causes (e.g. weather changes, site specific shading, sensor noise, see 3.1 earlier)

597 and water flux imposed by the flux step. The challenge for the accurate detection of amplitudes

598 and phases is to maximize the extracted signal induced by the change in the water flux and to

599 minimize the "noise" with frequencies other than diel in the forcing temperature data.

600 Figures 9b and 9c show vertical velocities and thermal diffusivities quantified with Equations 10

601 and 12 after applying the different signal processing techniques outlined in the methods section.

602 The results clearly show that general temperature non-stationarity significantly 'leaks' into the

603 velocity results. The WFT is revealed as the worst performing technique with apparent velocity

604 variations of similar magnitude to the actual velocity step that is to be identified. This is due to

605 the shortness of the 1-day window selected to maximize the detection of the timing of the

606 velocity transients. Increasing the window would increase the method's accuracy during steady

607   velocity periods, but at the expense of reducing its ability to accurately delineate the step change.

608   The technique with best performing amplitudes and phase extraction is the zero-phase forward-

609   backward filter (*filtfilt* in Matlab), originally proposed by Hatch et al. [2006]. However, this

610   method still smooths the velocity transient (Figure 9b), and produces an apparent jump in

611   thermal diffusivity (Figure 9c), caused by the window length. By contrast DHR, which has been

612   attributed with robust detection of harmonics embedded in non-stationary signals [Vogt et al.,

613   2010; Gordon et al., 2012], exhibits significant noise in our test (Figures 7b and 7c). Our results

614   confirm what McCallum et al. [2012] had observed in their field application, mainly that heat

615   tracing results should not be trusted during times when the flux is expected to be transient. We

616   suggest that thermal diffusivity jumps in field data indicate times when the vertical flux is highly

617   transient or when erosion-depositional processes occur. However, as both would occur during

618   transient conditions it would be difficult to disentangle real changes in sensor spacing (as a

619   proxy for scour/depositional processes) from anomalies induced by transient velocities (Figures

620   5-8).

621   Figure 9 also demonstrates that there is a lower limit to the detection of velocity changes. This

622   limit depends on the signal-to-noise ratio, the ratio between temperature signal non-stationarity

623   caused by the transient water flux and other sources of non-stationarity. Fourier based signal

624   processing methods are prone to leakage between different frequencies. Leakage can obscure the

625   harmonic signal of interest, depends on the filter parameters and is difficult to quantify. The

626   forcing temperature may contain many simultaneous sources of non-stationarity with different

627   frequencies and magnitudes buried in the diel temperature records (e.g. caused by the local

628   climate, seasonal shading, surface flow, etc.). Therefore, the detectability of transient flux

629   magnitudes will depend on the strength of non-stationarity from other sources. In some cases it

630   may become impossible to disentangle the diel frequency from other sources of non-stationarity.

631   Our results illustrate that while signal processing is mandatory to extract harmonic amplitude

632   and phases its limited ability to deal with signal non-stationarity thwarts the accurate delineation

633   of transient fluxes and thermal diffusivities or sediment scour/deposition.

634   McCallum et al. [2012] observed that the thermal diffusivities calculated from heat tracing can

635   temporarily exceed any physically plausible limits. Further, they warned that this could be due to

636   violated boundary conditions for the analytical solution. Here, we show that the apparent

637   "jumps" in thermal diffusivity originate from signal processing artifacts caused by transient

638   water fluxes that impose sudden non-stationarity on the underlying temperature signal. These

signal features are too fast for methods that make use of Fourier based time-frequency transformation and are thus incorrectly delineated.

In a different study, Luce et al. [2013] proposed that streambed scouring could be inferred from quantifications of apparent variation in sensor spacing Δz, rather than thermal diffusivity. Tonina et al. [2014] tested the quantification of time-variant scour and deposition with analytical heat tracing in combination with DHR and Equations 9-11. While they tested the method's capability by manually changing the amount of sediment above the buried temperature sensor during times when the flux was relatively steady, naturally occurring sediment movement typically occurs when the stream discharge is high. This implies transient stream discharge conditions which are also the main driver for transient vertical fluxes. Gariglio et al. [2014] attributed highly variable thermal diffusivities with values exceeding physically plausible limits, as calculated during times of transient river discharge using DHR, to sediment scour/deposition. We point out that quantifying naturally occurring sediment movement, such as scour and depositional processes, using analytical heat tracing may be a challenging proposition. This is because a) the derivation for sensor spacing is the same but rearranged equation as that for thermal diffusivity (Equations 10 and 11) and results are prone to artifacts as illustrated earlier, and b) the natural example presented in Luce et al. [2013] suggests that the water flux was transient as indicated by the fluctuating river discharge data. Flux and diffusivity artifacts arising from signal non-stationarity, which are to be expected during transient discharge conditions when sediment movement likely occurs simultaneously, could thus easily be mistaken for scour/depositional processes. We demonstrate that heat tracing based on harmonic signals becomes increasingly unsuitable to quantify vertical fluxes, thermal diffusivities or sediment scour/deposition from temperature data under increasingly transient flow conditions.

Sediment temperature data reported in the literature and acquired during highly transient hydraulic events (e.g. floods) at the system boundary exhibit high non-stationarity in regards to harmonic components (e.g. see Barlow et al. [2009]; Mutiti and Levy [2010]). We expect that the risk of leakage due to signal time-frequency transformation, and associated impact on amplitude and phase data, will contribute considerable uncertainty to the delineation of transient fluxes, thermal diffusivities or sediment scour/deposition. Furthermore, flux transients often occur on time scales less than one harmonic cycle (e.g. duration of flood peak, dam releases or the onset or cessation of near-stream groundwater pumping). Consequently, to quantify highly transient fluxes and thermal diffusivity or sediment scour/deposition under such conditions we recommend that numerical approaches be deployed [e.g. Holzbecher, 2005; Voytek et al., 2013],

672   or that methods based on signal processing techniques offering improved delineation of transient

673   processes from frequency-domain data are deployed or developed.

4. Conclusion

A thorough analysis of Stallman's [1965] analytical solution reveals that changes in the vertical water flux induce non-stationarity in the temperature signal during its propagation. The severity of non-stationarity depends on the magnitude of the flux transient. A simulated worst case water velocity transient (step change from 0 to -1 m/d with harmonic amplitude of 3 ºC) triggers an abrupt transition to non-stationarity in the sediment temperature signal. The response (difference between modeled temperature and analytical solution assuming steady-state velocity) depends on the thermal diffusivity and the onset of the velocity step change relative to the phase of the harmonic temperature boundary. The maximum response is ~2.3 ºC and return to stationarity occurs within 1 harmonic cycle (= 1 day) for physically plausible sediment thermal diffusivities in the range of 0.02-0.13 m^2/d.

Inverting transient vertical fluxes and thermal diffusivities from temperature records using analytical heat tracing relies either on the transformation of the signal from time to frequency domain, or extraction of time-variable amplitude and phase information of a fixed-frequency harmonic. Both are only possible with signal processing techniques. We benchmarked the ability of four commonly used signal processing methods (windowed Fourier transform (WFT), forward-backward zero phase filter (filtfilt), continuous wavelet transform (CWT) and dynamic harmonic regression (DHR)) to delineate signal non-stationarity implicit in the temperature-time signal. This was done by numerically simulating the transient advective thermal velocity with a harmonic temperature boundary and comparing the known to the inverted velocities obtained by the signal processing and the analytical solution. All the signal processing techniques were shown to offer poor time-domain resolution of frequency-domain features, and to erroneously spread amplitude and phase information across up to approx. 4 harmonic cycles (4 days). There is a technique and parameter dependent trade-off between magnitude and duration of the response to abrupt signal non-stationarity.

In essence, our analysis shows that the ability to accurately resolve flux transients with analytical heat tracing is currently limited by the signal processing, rather than the assumption of steady-state flow inherent to Stallman's [1965] analytical solution. This is because local signal stationarity is assumed for each extracted amplitude and/or phase value. The signal processing response appears to be independent of the advective thermal velocity step size, including reversal, for steps smaller than ±1 m/d. The match between modeled and inverted velocities improves with decreasing rates of velocity change. Implications on heat tracing are that: a) a sudden sharp transient in apparent velocity appears smoothed and earlier than the hydraulic

25

707   driver, and b) an apparent thermal diffusivity overshoot (undershoot) for a downward (upward)

708   velocity change with values that can exceed physically plausible limits. The latter is caused by

709   signal processing methods introducing phase artifacts originating from response to signal non-

710   stationarity. While the thermal diffusivity anomaly can be used as an indication of a flux

711   transient (including direction), the quantified flux and diffusivity values or sensor spacing

712   (sediment scour/deposition) should not be trusted during that time.

713   Real-world temperature records contain non-stationarities caused by a range of different

714   superimposed factors, such as abrupt hydrologic or meteoric changes, or anthropogenic

715   disturbances. We applied the commonly used heat tracing techniques to numerically simulated

716   streambed temperatures with the model driven by previously presented surface water

717   temperature data [Rau et al., 2010] as the upper boundary. Inversion of fluxes and thermal

718   diffusivities from the simulated temperatures reveals that, besides the erroneous temporal

719   spreading of the flux transient (time-smearing), there are anomalies in the diffusivity results that

720   originate from the signal processing techniques. The forward-backward zero-phase filter was

721   identified as the best-performing amplitude and phase extraction method causing the least

722   artifacts, but limited to producing 2 flux results per day.

723   Our results have significant implications for the practical application of inverting water fluxes,

724   thermal diffusivities or sensor spacing (scour/deposition) from temperature data using

725   increasingly popular methods that are based on harmonically forced analytical solutions. While

726   these techniques are useful to estimate fluxes during times when hydraulic drivers indicate

727   steady-state conditions, attention must be paid during transient conditions. This suggests that,

728   when highly transient fluxes are to be calculated from temperature records, hydraulic heads

729   should be monitored alongside temperature data, and that either numerical methods or new

730   signal processing methods extracting features in the time domain must be applied. Besides the

731   implications for heat tracing in near-surface water systems, our results point out that the

732   response of signal processing techniques to non-stationary data must be carefully considered

733   when time-varying physical processes are inferred from frequency-domain information in other

734   geophysical datasets.

References

Anderson, M. P. (2005), Heat as a Ground Water Tracer, *Ground Water*, *43*(6), 951-968, doi: 10.1111/j.1745-6584.2005.00052.x.

Barlow, J. R. B., and R. H. Coupe (2009), Use of heat to estimate streambed fluxes during extreme hydrologic events, *Water Resources Research*, *45*, W01403, doi: 10.1029/2007WR006121.

Best, A. I., C. McCann, and J. Sothcott (1994), The relationships between the velocities, attenuations and petrophysical properties of reservoir sedimentary rocks1, *Geophysical Prospecting*, *42*(2), 151-178, doi: 10.1111/j.1365-2478.1994.tb00204.x.

Constantz, J. (2008), Heat as a tracer to determine streambed water exchanges, *Water Resources Research*, *44*, -, doi: 10.1029/2008WR006996.

COMSOL (2014), COMSOL Multiphysics Version 5, COMSOL Inc., Burlington, MA, USA.

Cuthbert, M. O. (2010), An improved time series approach for estimating groundwater recharge from groundwater level fluctuations, *Water Resources Research*, *46*(9), W09515, doi: 10.1029/2009WR008572.

Cuthbert, M. O., and R. Mackay (2013), Impacts of nonuniform flow on estimates of vertical streambed flux, *Water Resources Research*, *49*(1), 19-28, doi: 10.1029/2011WR011587.

Cuthbert, M. O., R. Mackay, V. Durand, M.-F. Aller, R. B. Greswell, and M. O. Rivett (2010), Impacts of river bed gas on the hydraulic and thermal dynamics of the hyporheic zone, *Advances in Water Resources*, *33*, 1347-1358, doi: 10.1016/j.advwatres.2010.09.014.

27

766   Erickson, J. (2014), Continuous wavelet transform and inverse, Matlab Central,

767   <http://www.mathworks.com/matlabcentral/fileexchange/20821-continuous-wavelet-transform-

768   and-inverse>, updated: 14/10/2014, accessed: Jan 2015.

769   Fanelli, R. M., and L. K. Lautz (2008), Patterns of water, heat, and solute flux through

770   streambeds around small dams., *Ground Water*, *46*, 671-687, doi: 10.1111/j.1745-

771   6584.2008.00461.x.

772   Gordon, R. P., L. K. Lautz, M. A. Briggs, and J. M. McKenzie (2012), Automated calculation of

773   vertical pore-water flux from field temperature time series using the VFLUX method and

774   computer program, *Journal of Hydrology*, *420-421*, 142-158, doi:

775   10.1016/j.jhydrol.2011.11.053.

776   Goto, S., M. Yamano, and M. Kinoshita (2005), Thermal response of sediment with vertical

777   fluid flow to periodic temperature variation at the surface, *J Geophys Res-Sol Ea*, *110*, B01106,

778   doi: 10.1029/2004JB003419.

779   Gariglio, F. P., D. Tonina, and C. H. Luce (2013), Spatiotemporal variability of hyporheic

780   exchange through a pool-riffle-pool sequence, *Water Resources Research*, *49*(11), 7185-7204,

781   doi: 10.1002/wrcr.20419.

782   Harris, F. J. (1978), On the use of windows for harmonic analysis with the discrete Fourier

783   transform, *Proceedings of the IEEE*, *66*(1), 51-83, doi: 10.1109/PROC.1978.10837.

784   Hatch, C. E., A. T. Fisher, J. S. Revenaugh, J. Constantz, and C. Ruehl (2006), Quantifying

785   surface water–groundwater interactions using time series analysis of streambed thermal records:

786   Method development, *Water Resources Research*, *42*, W10410, doi: 10.1029/2005WR004787.

787   Havin, V., and B. Jöricke (1994), *The uncertainty principle in harmonic analysis*, Springer.

788   Holzbecher, E. (2005), Inversion of temperature time series from near-surface porous sediments,

789   *Journal of Geophysics and Engineering*, *2*, 343-348, doi: 10.1088/1742-2132/2/4/S07.

790   Irvine, D. J., R. H. Cranswick, C. T. Simmons, M. A. Shanafield, and L. K. Lautz (2015), The

791   effect of streambed heterogeneity on groundwater-surface water exchange fluxes inferred from

792   temperature time series, *Water Resources Research*, n/a-n/a, doi: 10.1002/2014WR015769.

793   Jensen, J. K., and P. Engesgaard (2011), Nonuniform Groundwater Discharge across a

794   Streambed: Heat as a Tracer, *Vadose Zone J*, *10*, 98, doi: 10.2136/vzj2010.0005.

795 Keery, J. S., and A. Binley (2007), Temperature measurements for determining groundwater–

796 surface water fluxes, *Rep. Science Report SC030155/SR9*, Environment Agency & Lancaster

797 University, Bristol, UK.

798 Keery, J., A. Binley, N. Crook, and J. W. N. Smith (2007), Temporal and spatial variability of

799 groundwater–surface water fluxes: Development and application of an analytical method using

800 temperature time series, *Journal of Hydrology*, *336*, 1-16, doi: 10.1016/j.jhydrol.2006.12.003.

801 Lautz, L. K. (2010), Impacts of nonideal field conditions on vertical water velocity estimates

802 from streambed temperature time series, *Water Resources Research*, *46*, W01509, doi:

803 10.1029/2009WR007917.

804 Lautz, L. K. (2012), Observing temporal patterns of vertical flux through streambed sediments

805 using time-series analysis of temperature records, *Journal of Hydrology*, *464–465*, 199–215, doi:

806 10.1016/j.jhydrol.2012.07.006.

807 Luce, C. H., D. Tonina, F. Gariglio, and R. Applebee (2013), Solutions for the diurnally forced

808 advection-diffusion equation to estimate bulk fluid velocity and diffusivity in streambeds from

809 temperature time series, *Water Resources Research*, *49*(1), 488-506, doi:

810 10.1029/2012WR012380.

811 McCallum, A. M., M. S. Andersen, G. C. Rau, and R. I. Acworth (2012), A 1D analytical

812 method for estimating surface water groundwater interactions and effective thermal diffusivity

813 using temperature time series, *Water Resources Research*, *48*, W11532.

814 McCallum, A. M., M. S. Andersen, G. C. Rau, J. R. Larsen, and R. I. Acworth (2014), River-

815 aquifer interactions in a semiarid environment investigated using point and reach measurements,

816 *Water Resources Research*, *50*(4), 2815-2829, doi: 10.1002/2012WR012922.

817 Munz, M., S. E. Oswald, and C. Schmidt (2011), Sand box experiments to evaluate the influence

818 of subsurface temperature probe design on temperature based water flux calculation, *Hydrology*

819 *and Earth System Sciences Discussions*, *8*, 6155-6197, doi: 10.5194/hessd-8-6155-2011.

820 Mutiti, S., and J. Levy (2010), Using temperature modeling to investigate the temporal

821 variability of riverbed hydraulic conductivity during storm events, *Journal of Hydrology*, *388*,

822 321-334, doi: 10.1016/j.jhydrol.2010.05.011.

823 Onderka, M., S. Banzhaf, T. Scheytt, and A. Krein (2013), Seepage velocities derived from

824 thermal records using wavelet analysis, *Journal of Hydrology*, *479*(0), 64-74, doi:

825 10.1016/j.jhydrol.2012.11.022.

826 Oppenheim, A. V., R. W. Schafer, and J. R. Buck (1989), *Discrete-time signal processing*,

827 Prentice-hall Englewood Cliffs.

828 Pidlisecky, A., and R. Knight (2011), The Use of Wavelet Analysis to Derive Infiltration Rates

829 from Time-Lapse One-Dimensional Resistivity Records, *Vadose Zone*, *10*(2), 697-705, doi:

830 10.2136/vzj2010.0049.

831 Rau, G. C., M. S. Andersen, and R. I. Acworth (2012a), Experimental investigation of the

832 thermal dispersivity term and its significance in the heat transport equation for flow in

833 sediments, *Water Resources Research*, *48*, W03511, doi: 10.1029/2011WR011038.

834 Rau, G. C., M. S. Andersen, and R. I. Acworth (2012b), Experimental investigation of the

835 thermal time-series method for surface water-groundwater interactions, *Water Resources*

836 *Research*, *48*, W03530, doi: 10.1029/2011WR011560.

837 Rau, G. C., M. S. Andersen, A. M. McCallum, and R. I. Acworth (2010), Analytical methods

838 that use natural heat as a tracer to quantify surface water–groundwater exchange, evaluated using

839 field temperature records, *Hydrogeol J*, *18*, 1093-1110, doi: 10.1007/s10040-010-0586-0.

840 Roshan, H., G. C. Rau, M. S. Andersen, and I. R. Acworth (2012), Use of heat as tracer to

841 quantify vertical streambed flow in a two-dimensional flow field, *Water Resources Research*,

842 *48*(10), W10508, doi: 10.1029/2012WR011918.

843 Shanafield, M., C. Hatch, and G. Pohll (2011), Uncertainty in thermal time series analysis

844 estimates of streambed water flux, *Water Resources Research*, *47*, W03504, doi:

845 10.1029/2010WR009574.

846 Soto-López, C. D., T. Meixner, and T. P. A. Ferré (2011), Effects of measurement resolution on

847 the analysis of temperature time series for stream-aquifer flux estimation, *Water Resources*

848 *Research*, *47*, W12602, doi: 10.1029/2011WR010834.

849 Stallman, R. W. (1965), Steady One-Dimensional Fluid Flow in a Semi-Infinite Porous Medium

850 with Sinusoidal Surface Temperature, *J Geophys Res*, *70*, 2821-2827, doi:

851 10.1029/JZ070i012p02821.

852 Suzuki, S. (1960), Percolation Measurements Based on Heat Flow Through Soil with Special

853 Reference to Paddy Fields, *J Geophys Res*, *65*, 2883, doi: 10.1029/JZ065i009p02883.

854 Swanson, T. E., and M. B. Cardenas (2010), Diel heat transport within the hyporheic zone of a

855 pool-riffle-pool sequence of a losing stream and evaluation of models for fluid flux estimation

856 using heat, *Limnol. Oceanogr.*, *55*, 1741-1754, doi: 10.4319/lo.2010.55.4.1741.

857   Swanson, T. E., and M. B. Cardenas (2011), Ex-Stream: A MATLAB program for calculating

858   fluid flux through sediment–water interfaces based on steady and transient temperature profiles,

859   *Computers & Geosciences*, *37*, 1664-1669, doi: 10.1016/j.cageo.2010.12.001.

860   Tonina, D., C. Luce, and F. Gariglio (2014), Quantifying streambed deposition and scour from

861   stream and hyporheic water temperature time series, *Water Resources Research*, *50*(1), 287-292,

862   doi: 10.1002/2013WR014567.

863   Torrence, C., and G. P. Compo (1998), A practical guide to wavelet analysis, *Bulletin of the*

864   *American Meteorological society*, *79*(1), 61-78.

865   Vogt, T., P. Schneider, L. Hahn-Woernle, and O. A. Cirpka (2010), Estimation of seepage rates

866   in a losing stream by means of fiber-optic high-resolution vertical temperature profiling, *Journal*

867   *of Hydrology*, *380*, 154-164, doi: 10.1016/j.jhydrol.2009.10.033.

868   Voytek, E. B., A. Drenkelfuss, F. D. Day-Lewis, R. Healy, J. W. Lane, and D. Werkema (2013),

869   1DTempPro: Analyzing Temperature Profiles for Groundwater/Surface-water Exchange,

870   *Groundwater*, doi: 10.1111/gwat.12051.

871   Wörman, A., J. Riml, N. Schmadel, B. T. Neilson, A. Bottacin-Busolin, and J. E. Heavilin

872   (2012), Spectral scaling of heat fluxes in streambed sediments, *Geophysical Research Letters*,

873   *39*(23), L23402, doi: 10.1029/2012GL053922.

874   Wu, W., M. A. Geller, and R. E. Dickinson (2002), A case study for land model evaluation:

875   Simulation of soil moisture amplitude damping and phase shift, *Journal of Geophysical*

876   *Research: Atmospheres*, *107*(D24), 4793, doi: 10.1029/2001JD001405.

877   Young, P. C., D. J. Pedregal, and W. Tych (1999), Dynamic harmonic regression, *Journal of*

878   *Forecasting*, *18*, 369-394, doi: 10.1002/(SICI)1099-131X(199911)18:6<369::AID-

879   FOR748>3.0.CO;2-K.

Figure captions

881 Figure 1: Damping of amplitude (a) and shifting of phase (b) with depth for a sinusoid with
882 frequency of 1 cpd calculated using Stallman's [1965] analytical solution. Shaded areas
883 represent ranges based on effective thermal diffusivities $D_{min} = 0.02 \, m^2/d$, $D_{avg} = 0.075 \, m^2/d$
884 and $D_{max} = 0.13 \, m^2/d$ as reported in the literature [Shanafield et al., 2011; McCallum et al.,
885 2012]. Dashed horizontal lines show the depths at which temperature time-series were output
886 from the numerical model.

887 Figure 2: a) An example of multi-level temperature harmonics in response to a step change in
888 vertical water velocity as output from the numerical model. Here, Δz refers to sensor spacing of
889 0, 0.05, 0.2 and 0.4 m from the top of the sediment plotted with increasing intensity of black
890 color. The data serves to illustrate that a stationary harmonic is transformed into a non-stationary
891 harmonic through a transient in the vertical water velocity. b) Modeled multi-level temperature
892 data using real sediment temperature measurements at the streambed surface (from Rau et al.
893 [2010]) as a boundary for the same velocity as in a).

894 Figure 3: a) The thermal response to a transient water velocity: The temperature difference
895 between numerically modeled and analytically calculated harmonics due to a step change in
896 velocity from 0 to -1 m/d for $D_{min} = 0.02 \, m^2/d$, $D_{avg} = 0.075 \, m^2/d$ and $D_{max} = 0.13 \, m^2/d$ at
897 sensor spacing of $\Box z = 0.1$ and $\Box z = 0.2$ m. b) Same as a) but for the step change occurring at 8
898 different times (separated by 0.125 d or $\pi/4$) relative to the start of the harmonic temperature
899 signal used as boundary condition at $z = 0$ m (shown on right axis, with $D_{avg} = 0.075 \, m^2/d$ and
900 sensor spacing $\Box z = 0.2$ m.

901 Figure 4: Amplitude and phase response of common signal extraction methods (rows from top to
902 bottom: WFT, filtfilt, CWT and DHR) to the non-stationarity introduced by a step velocity
903 increase. Line color becomes lighter with increasing depth. Left column contains amplitudes,
904 right column contains phases. Note that the values obtained from filtfilt (c and d) are plotted
905 with dots whereas the lines are shown for visual improvement.

906 Figure 5: Vertical advective thermal velocities (left column: a, c, e, g) and thermal diffusivities
907 (right column: b, d, f, h) inverted using amplitudes and phases from peak picking applied to raw
908 data (red markers) as well as after applying 4 different signal processing methods (blue markers)
909 to the model temperature output. The different cases are in rows from top to bottom: 0 to -1 m/d

910   (a-b), 0 to 1 m/d (c-d), -1 m/d to 1 m/d (e-f), 1 m/d to -1 m/d (g-h). Refer to Figures 6 and 7 for

911   different velocity steps.

912   Figure 6: Downward advective thermal velocities (left column: a, c, e, g) and thermal

913   diffusivities (right column: b, d, f, h) inverted using amplitudes and phases from peak picking

914   applied to raw data (red markers) as well as after applying 4 different signal processing methods

915   (blue markers) to the model temperature output. The different cases are in rows from top to

916   bottom: 0 to -0.01 m/d (a-b), 0 to -0.1 m/d (c-d), 0 m/d to -0.5 m/d (e-f), 0 m/d to -5 m/d (g-h).

917   Figure 7: Upward advective thermal velocities (left column: a, c, e) and thermal diffusivities

918   (right column: b, d, f) inverted using amplitudes and phases from peak picking applied to raw

919   data (red markers) as well as after applying 4 different signal processing methods (blue markers)

920   to the model temperature output. The different cases are in rows from top to bottom: 0 to 0.1 m/d

921   (a-b), 0 to 0.5 m/d (c-d), 0 m/d to 2 m/d (e-f).

922   Figure 8: Vertical advective thermal velocities (left column: a, c, e, g) and thermal diffusivities

923   (right column: b, d, f, h) inverted using amplitudes and phases from peak picking applied to raw

924   data (red markers) as well as after applying 4 different signal processing methods (blue markers)

925   to the model temperature output. The different scenarios are a linear change of advective thermal

926   velocity from 0 to -1 m/d over a total time period of (in rows from top to bottom): 0.5 days (a-b),

927   1 day (c-d), 2 days (e-f) and 4 days (g-h).

928   Figure 9: a) Temperature output obtained from the numerical model at different depths (0, 0.05,

929   0.2 and 0.4 m from the top of the sediment) using measured surface water temperature data as

930   the top boundary (from Rau et al. [2010]). b) Advective thermal velocities and c) thermal

931   diffusivities inverted after the data has been processed with 4 different amplitude and phase

932   extraction methods.

933

Table captions

Table 1: Summary of maximum error and root mean square error (RMSE) calculated from modeled and inverted advective thermal velocities using unfiltered and filtered temperature data for the same magnitude velocity transients (0 to -1 m/d) but for different rates of velocity change. The values in this table represent a quantification of the results in Figure 8a, 8c, 8e, 8g and Figure 5a.

Table 2: Summary of maximum error and root mean square error (RMSE) calculated from modeled and inverted thermal diffusivities using unfiltered and filtered temperature data for the same magnitude velocity transients (0 to -1 m/d) but for different rates of velocity change. The values in this table represent a quantification of the results in Figure 8b, 8d, 8f, 8h and Figure 5b.
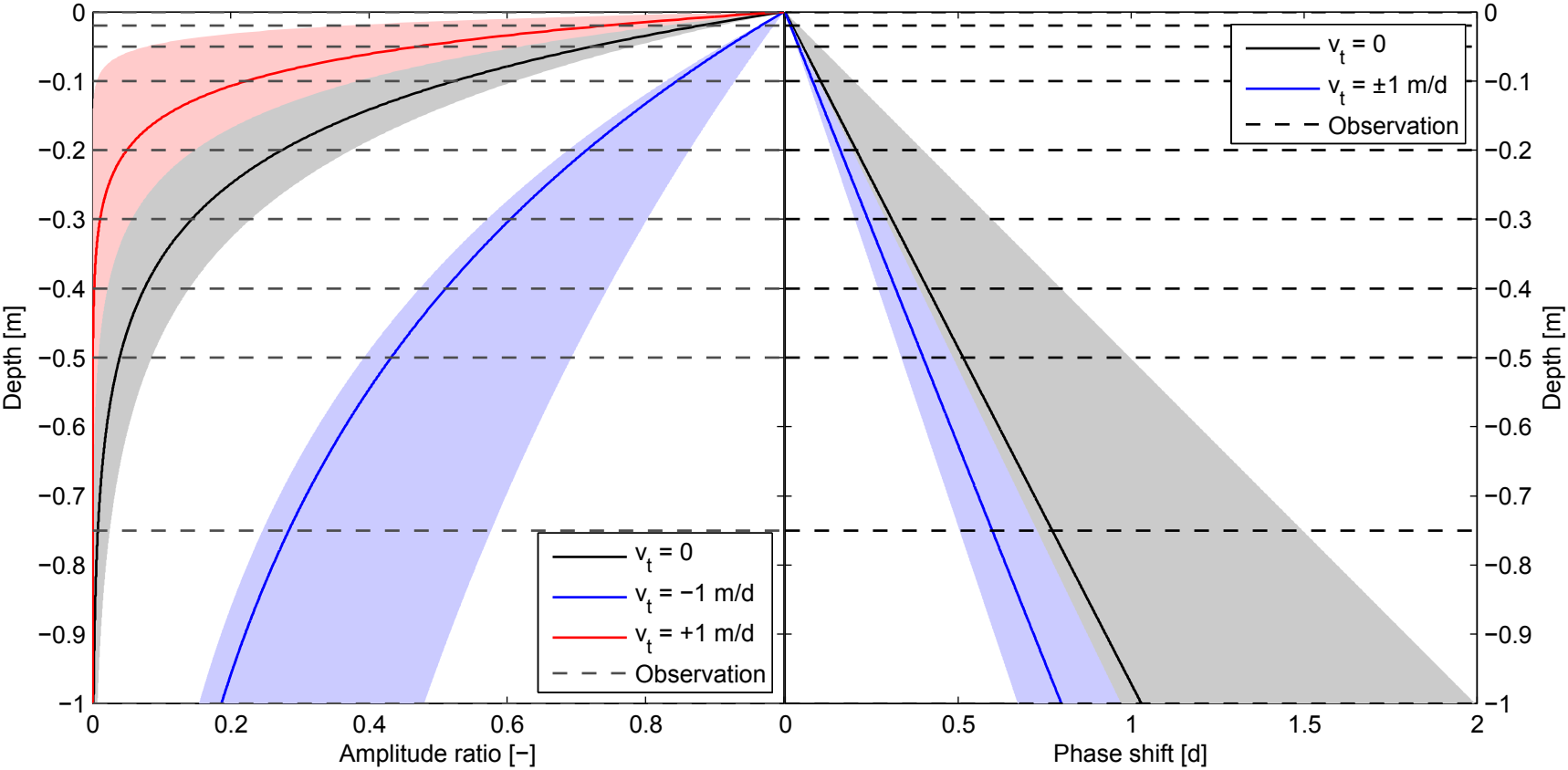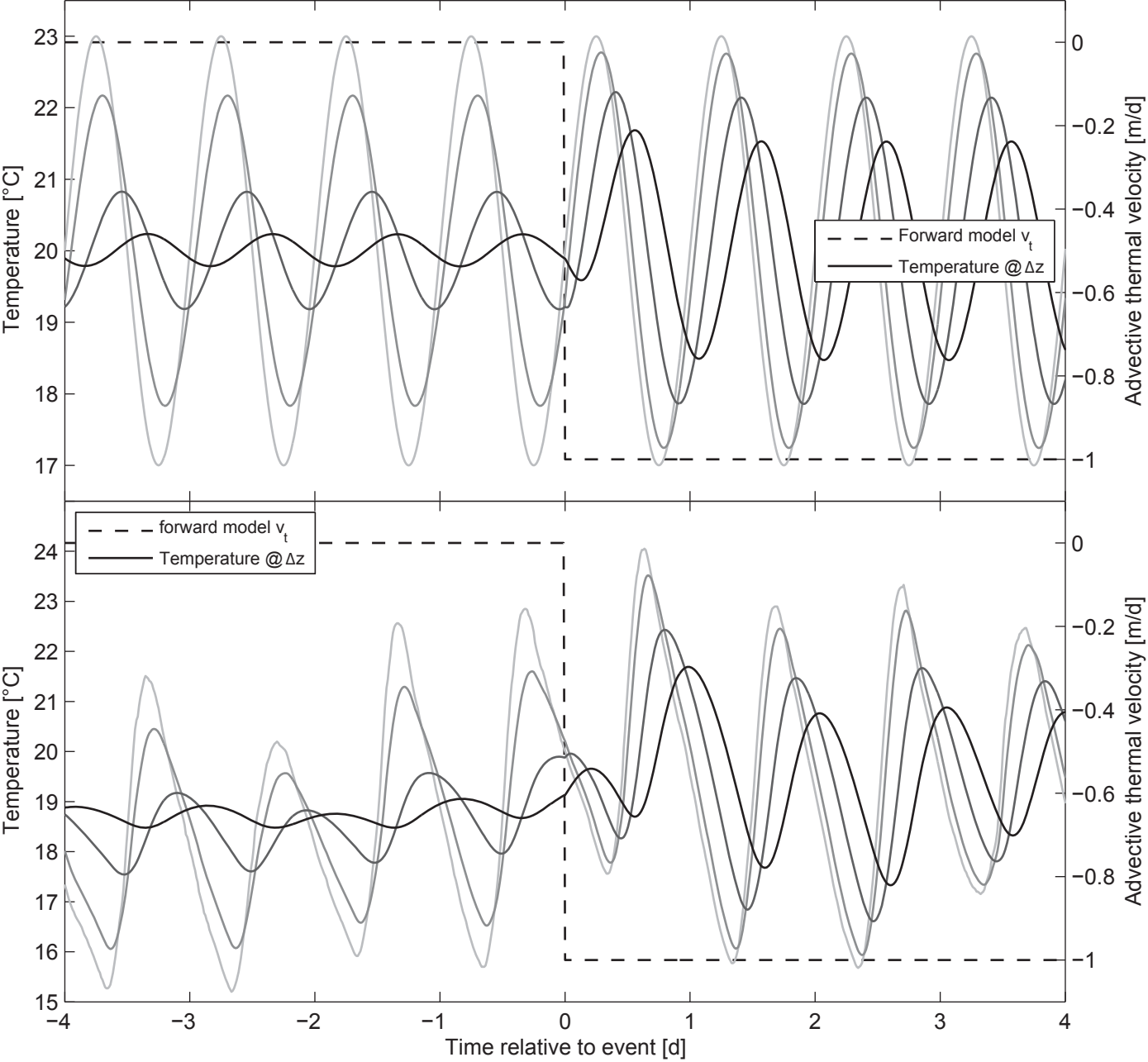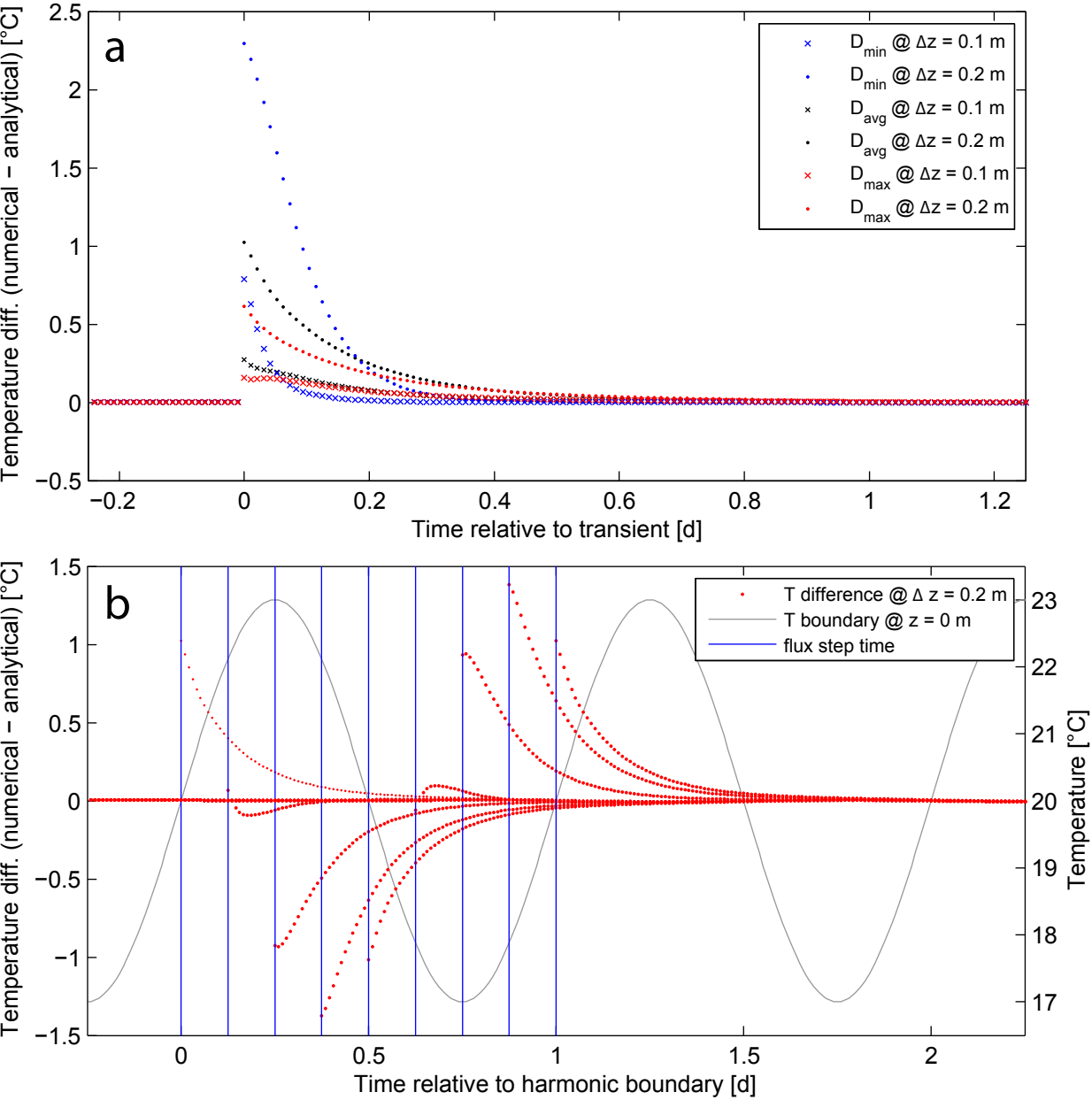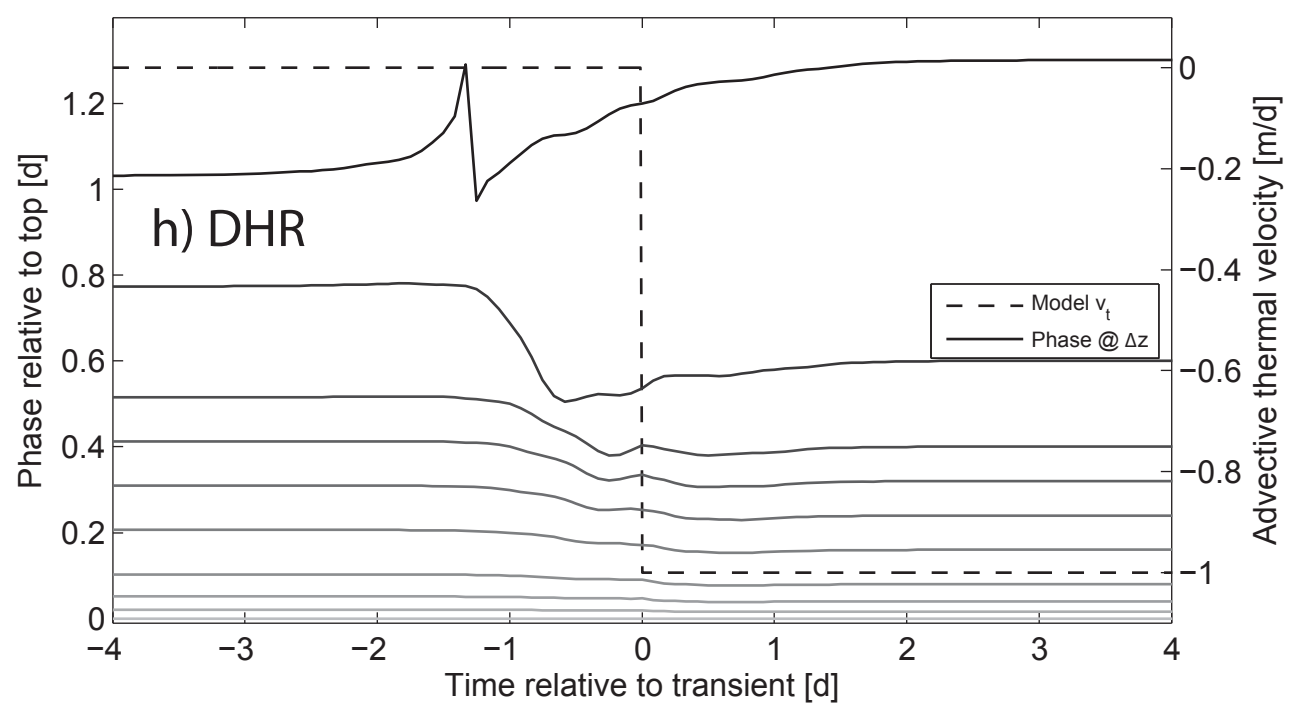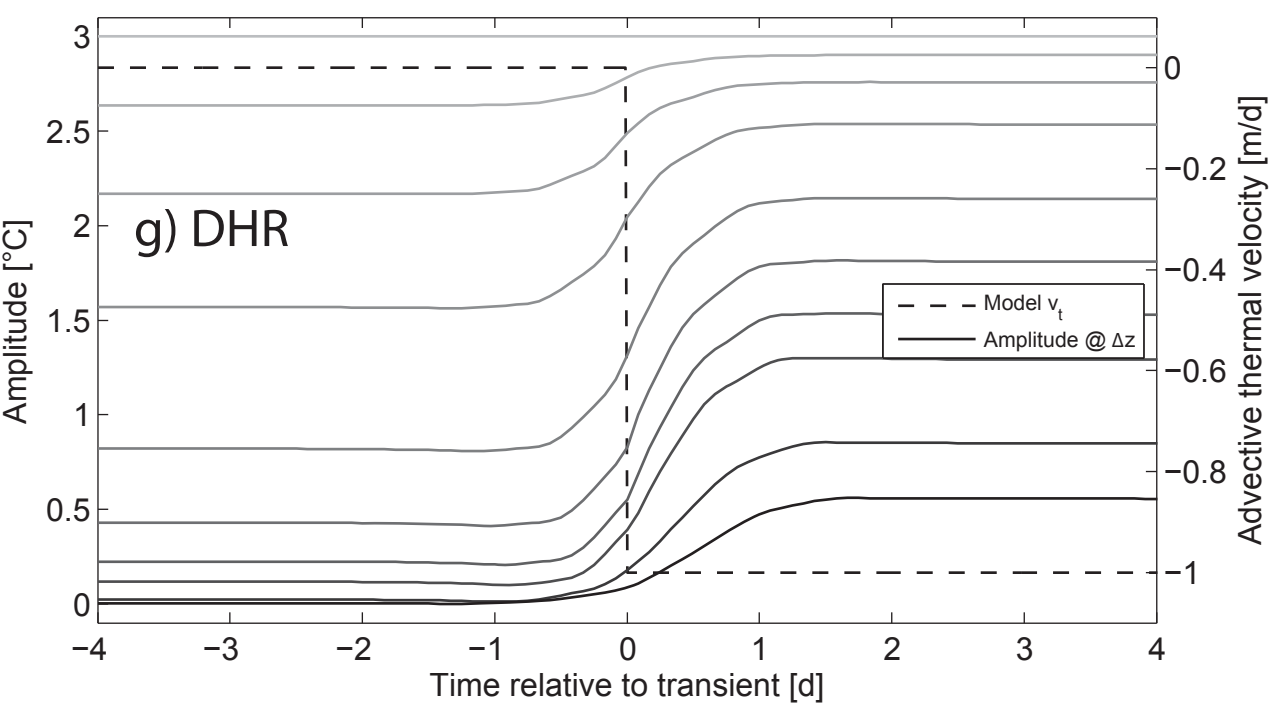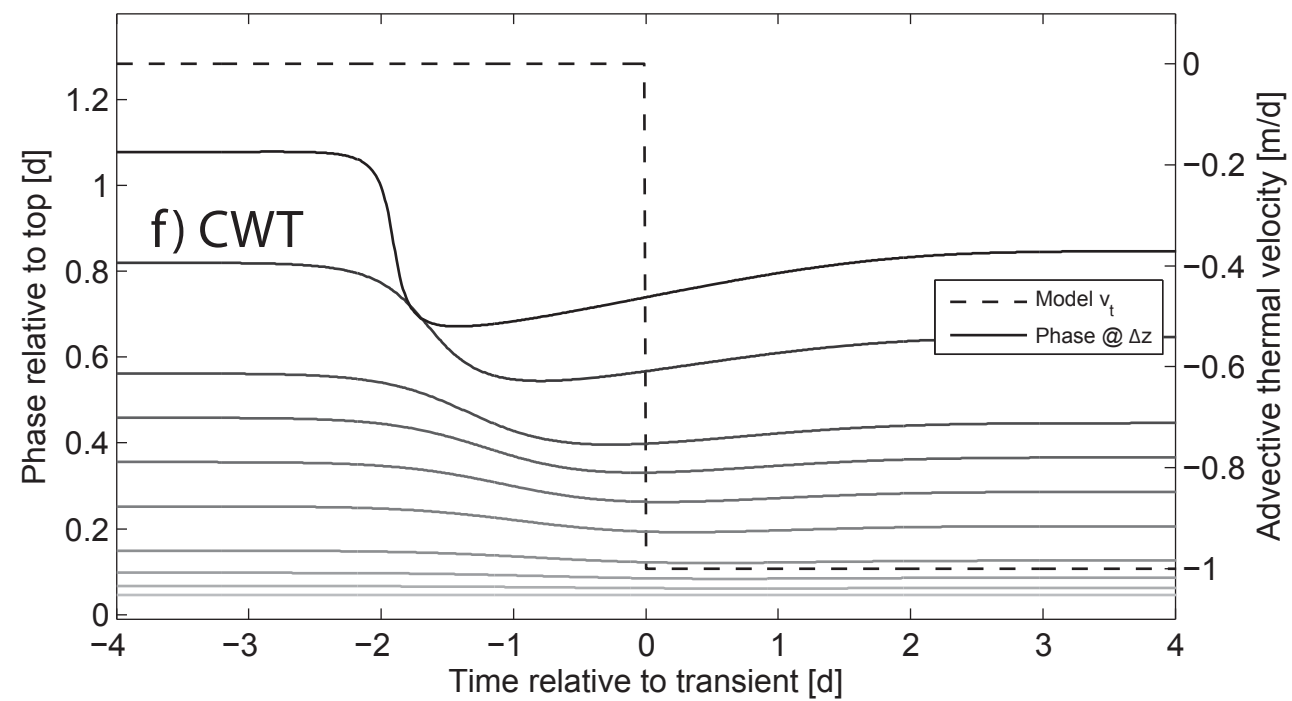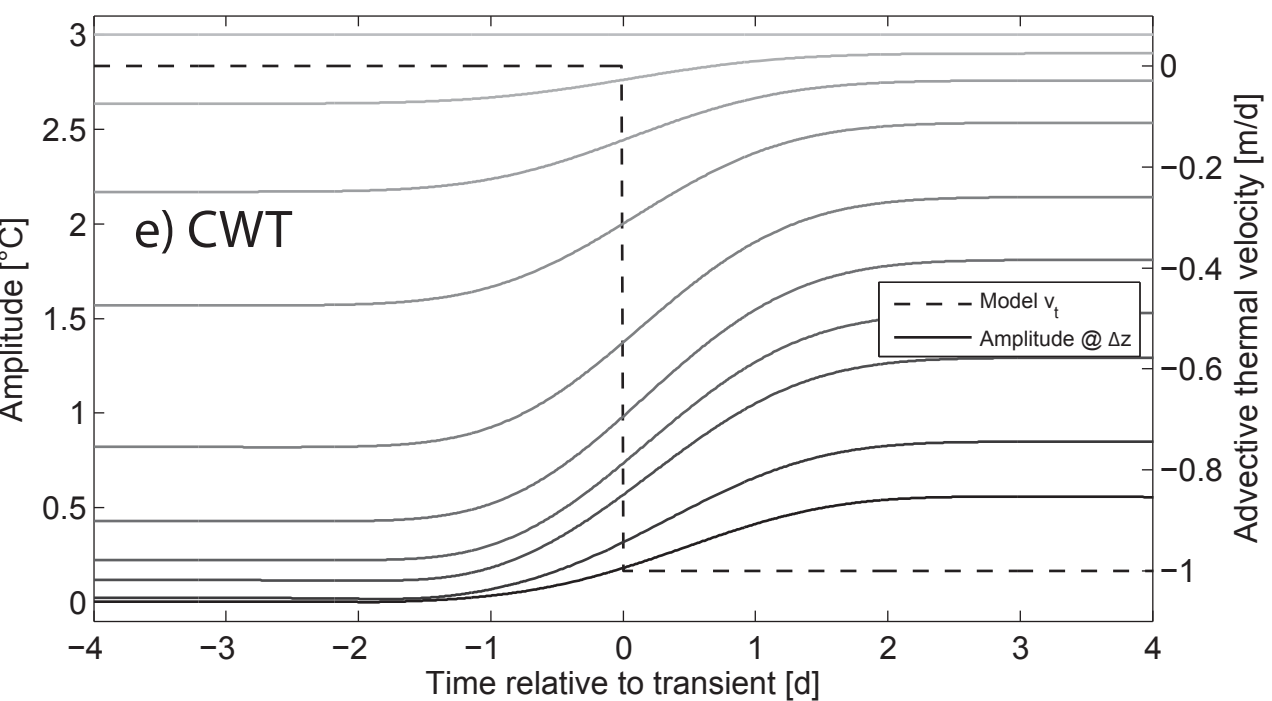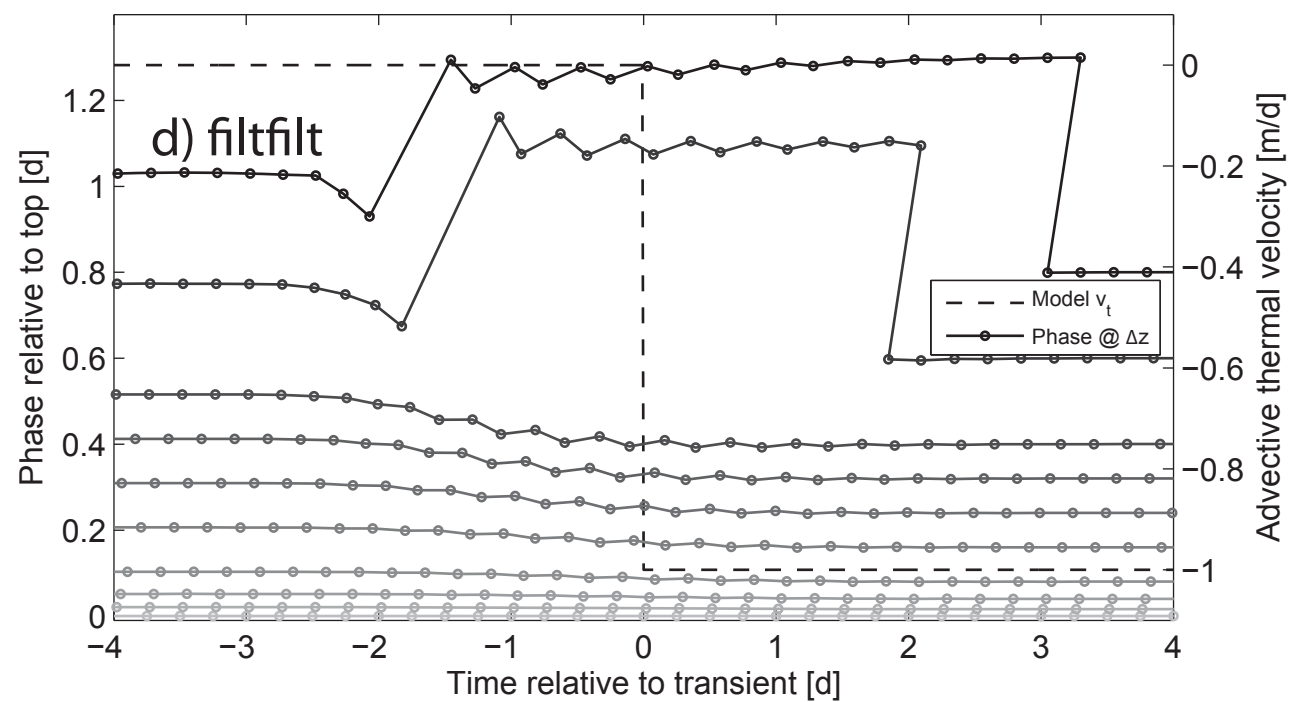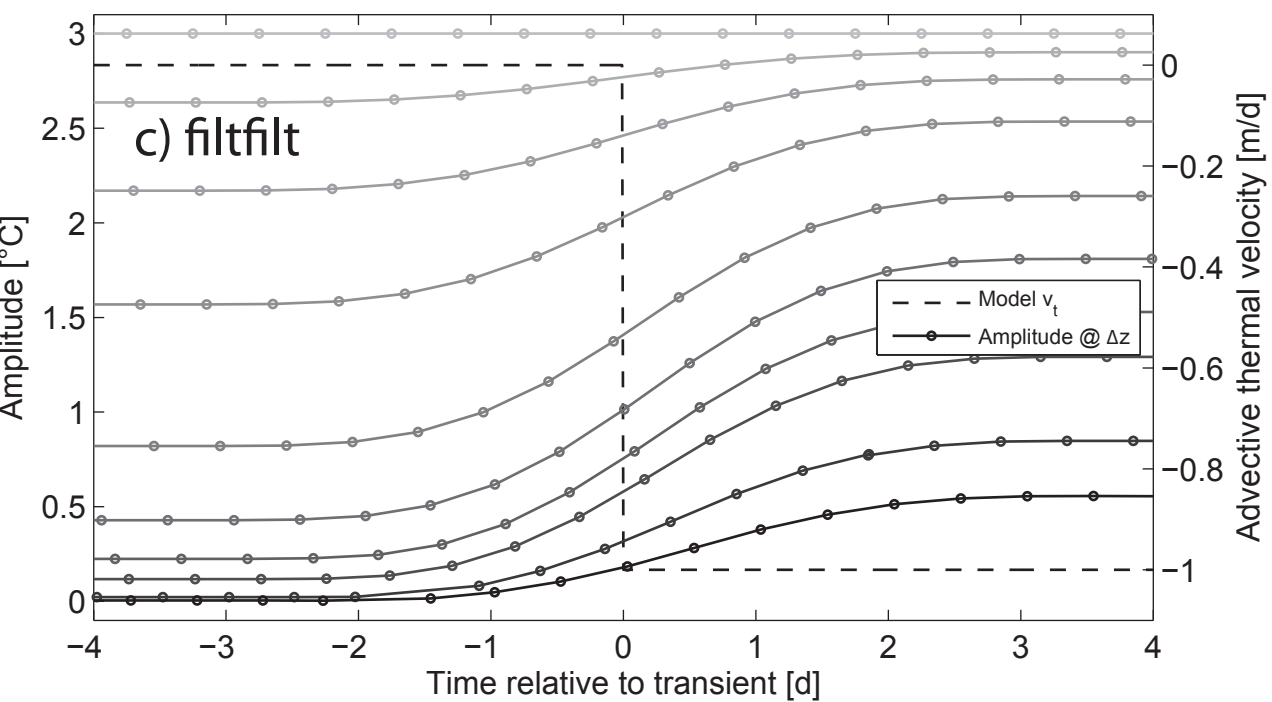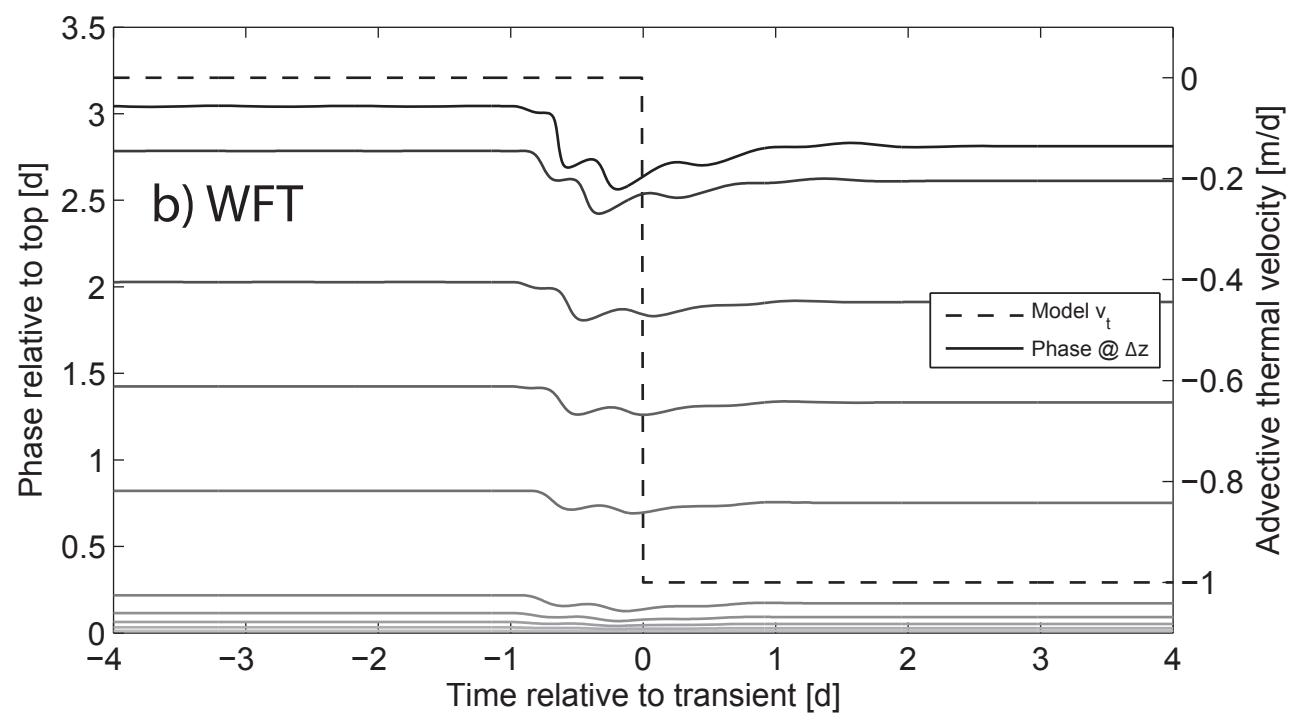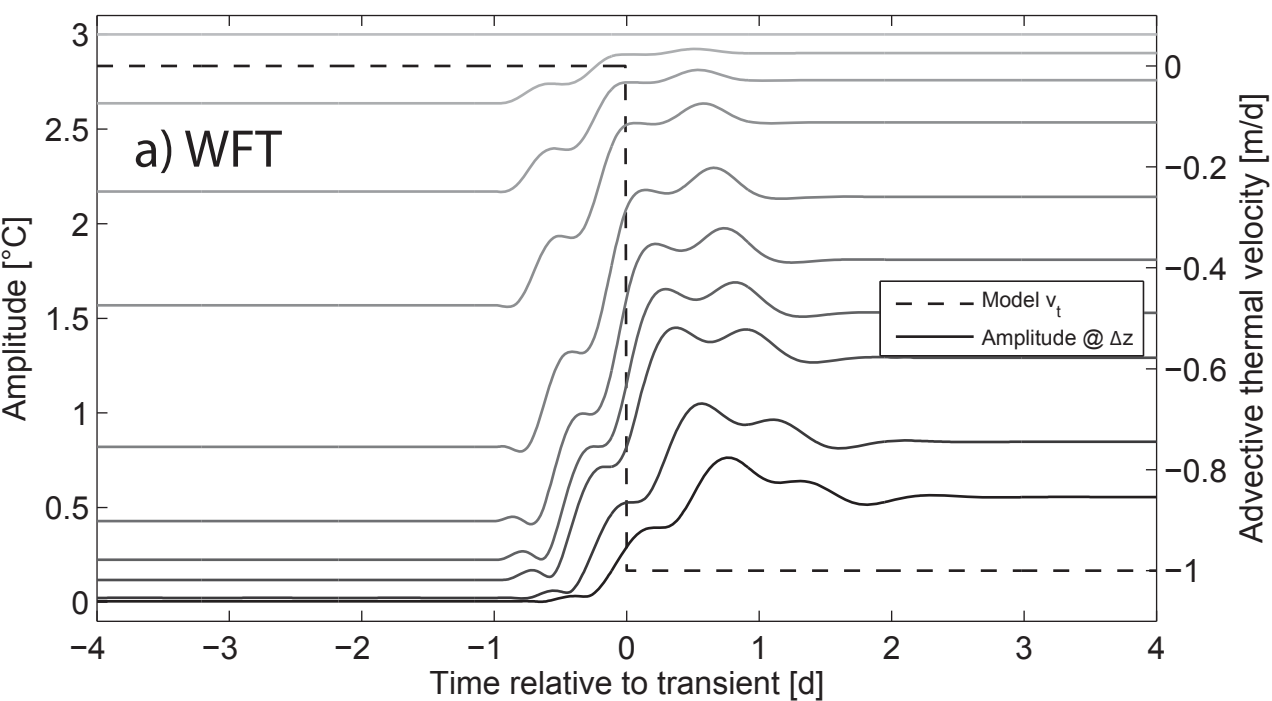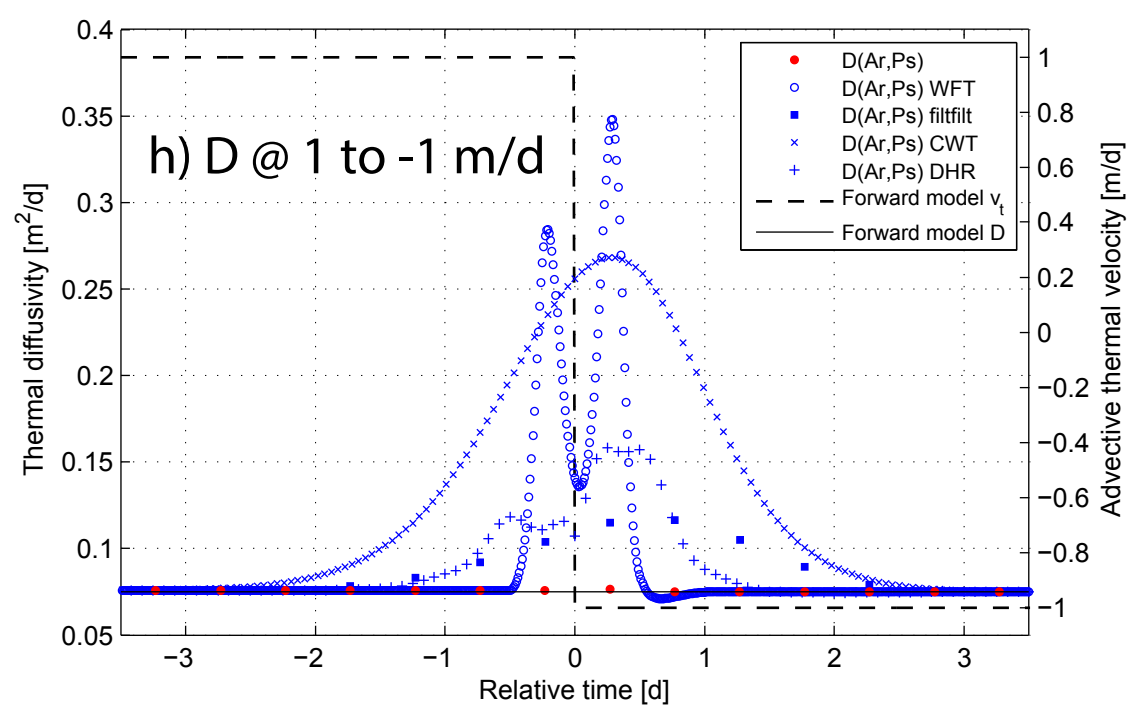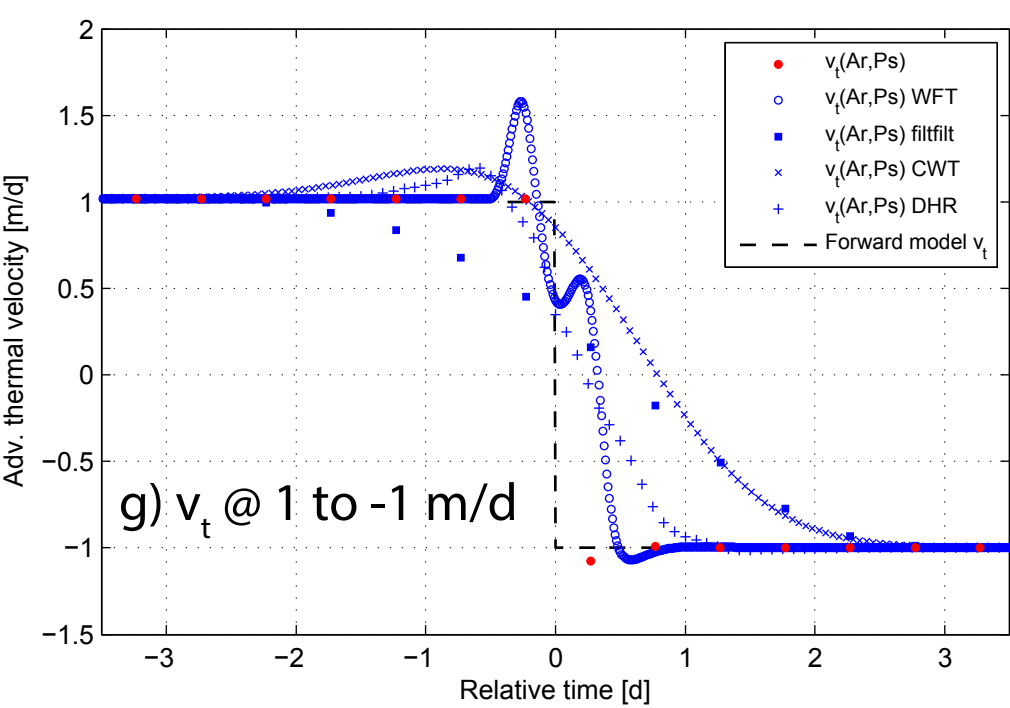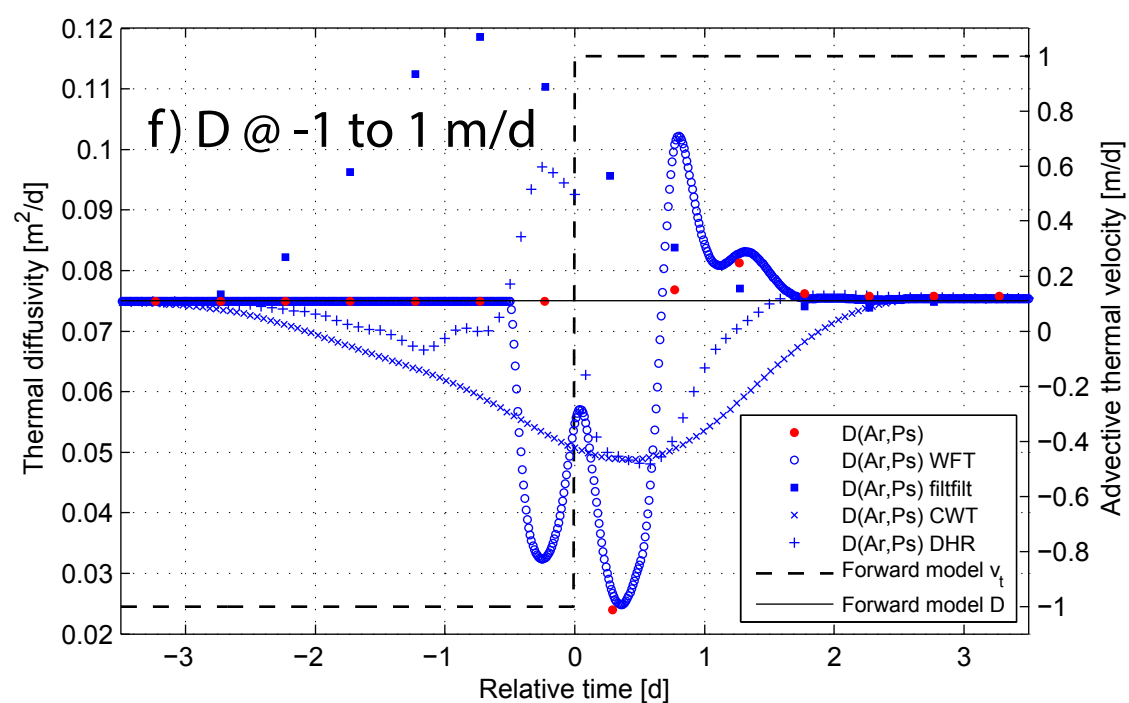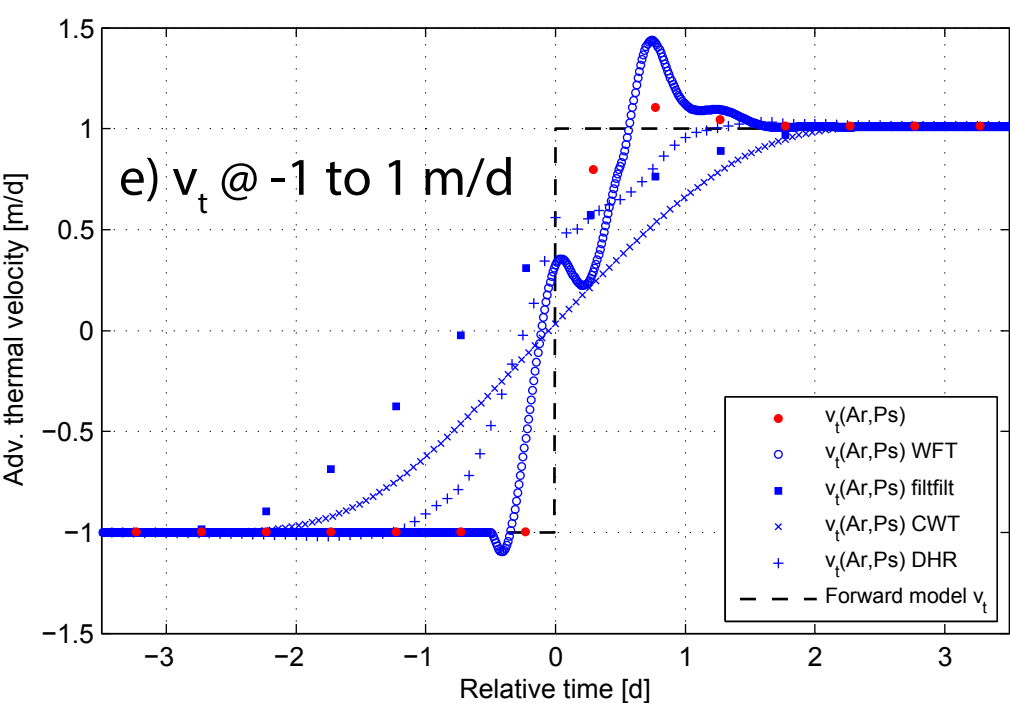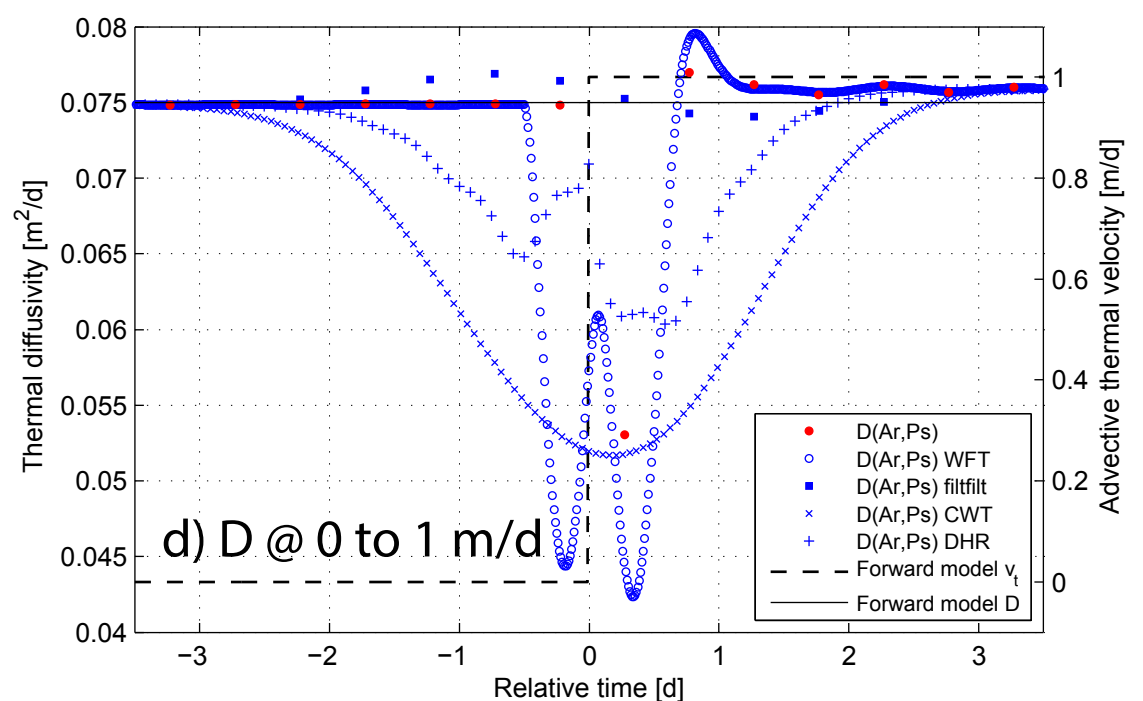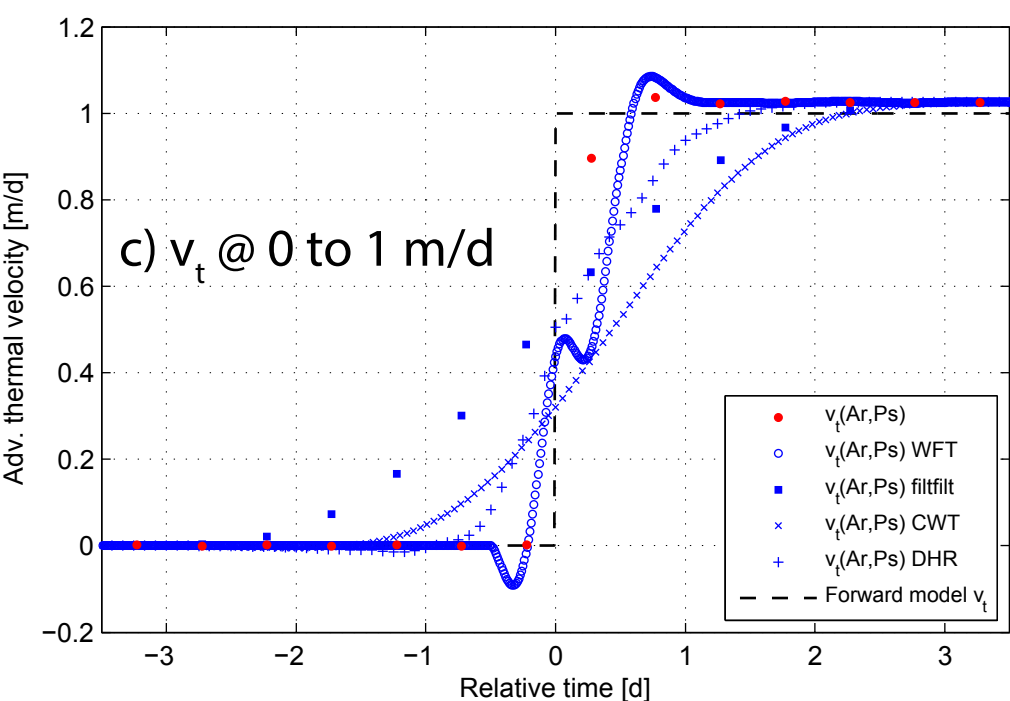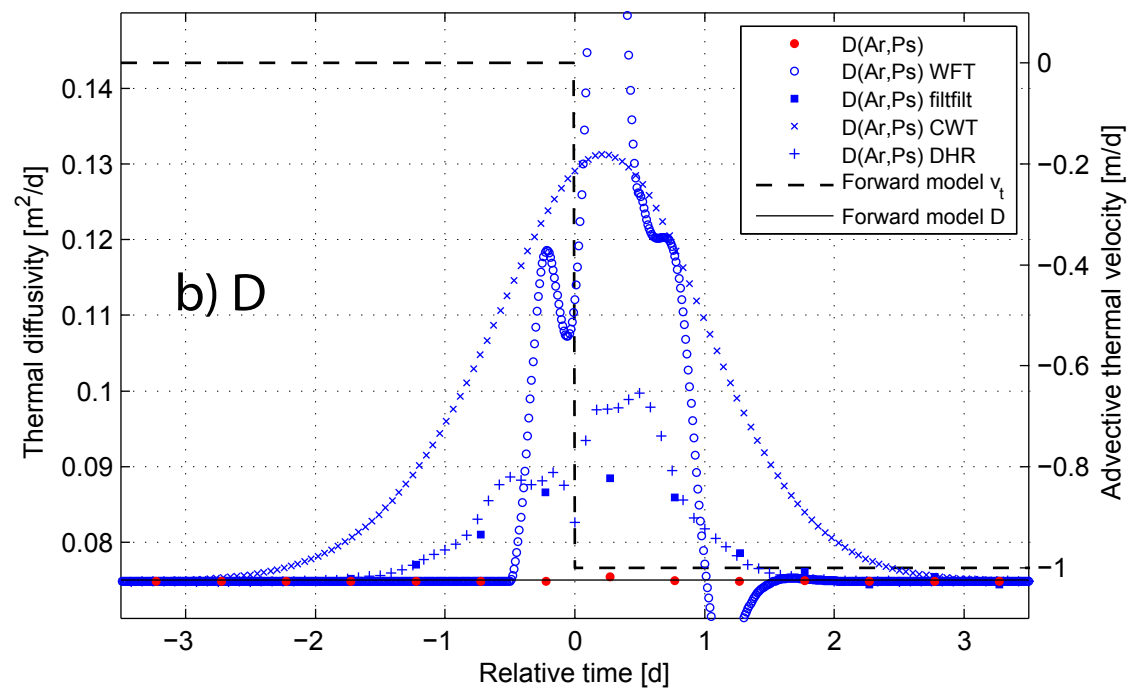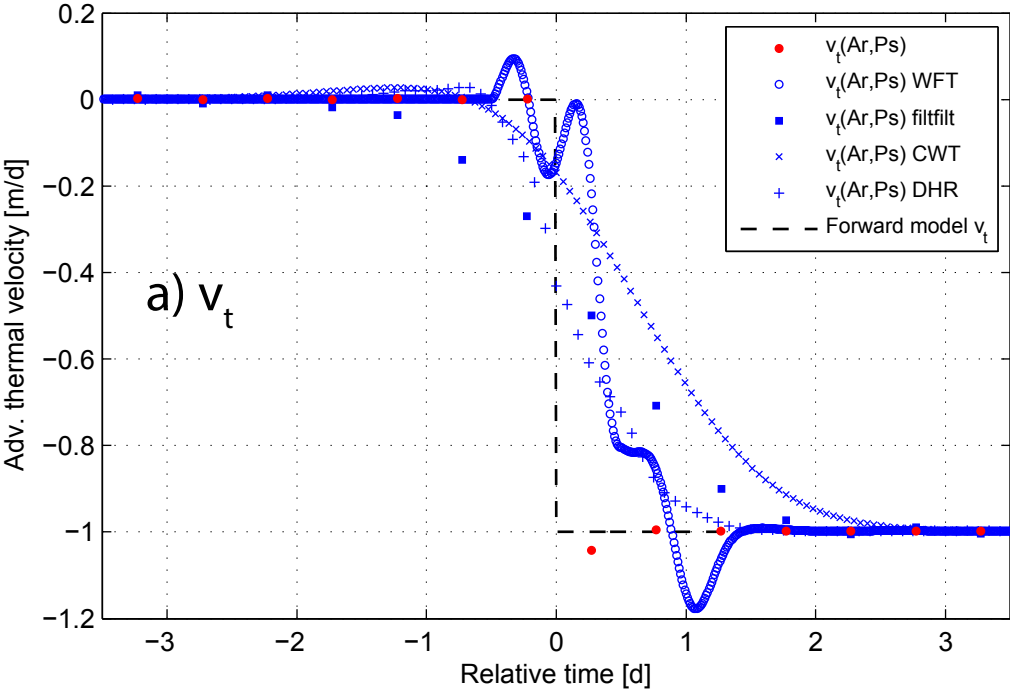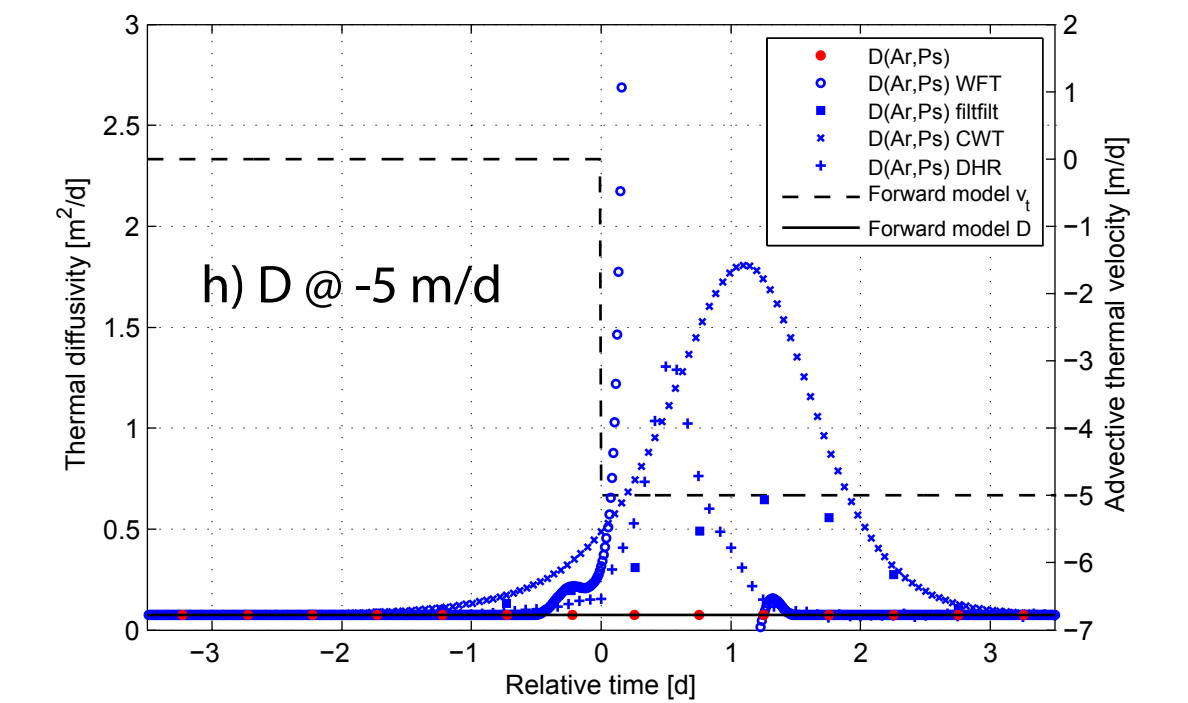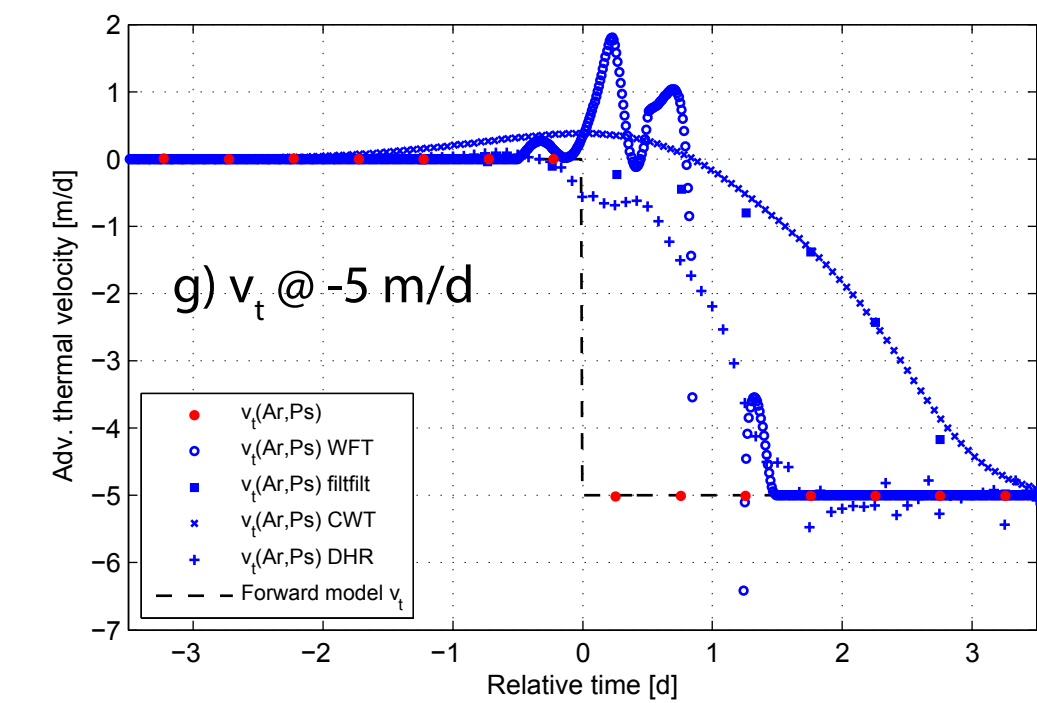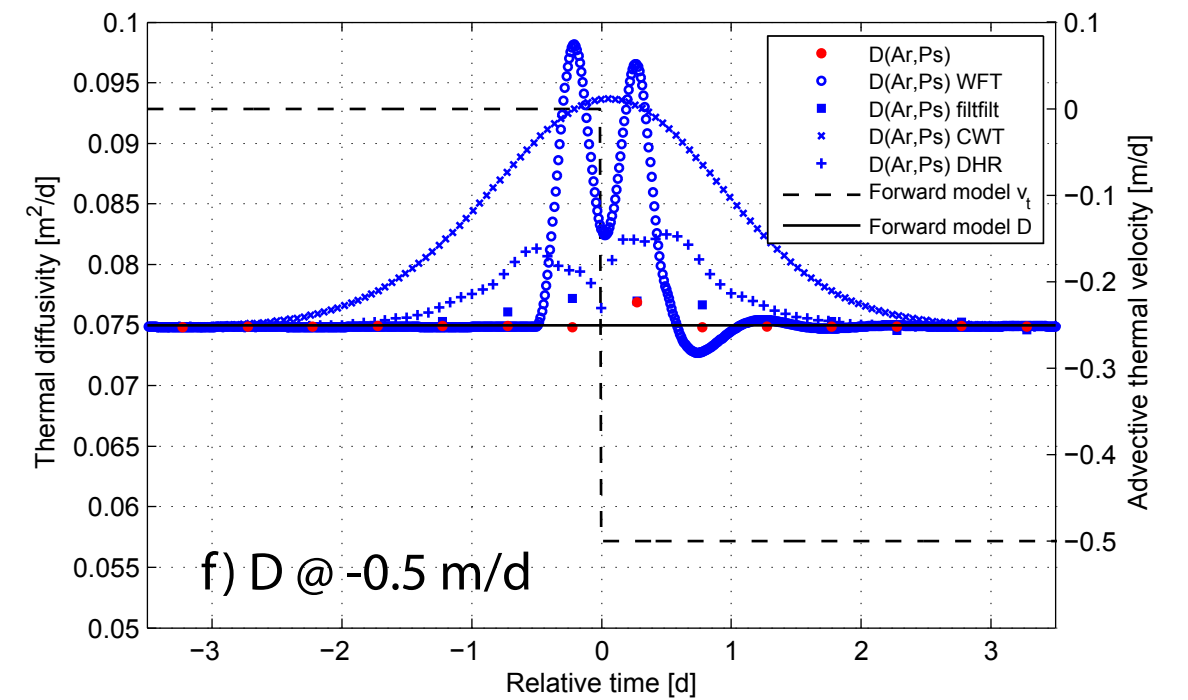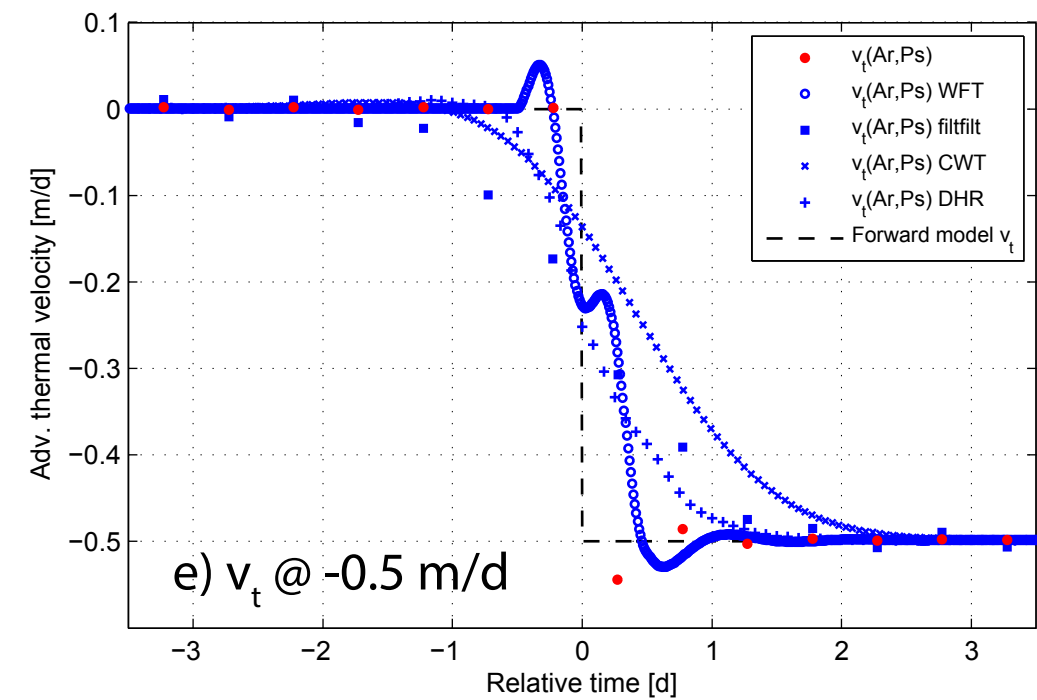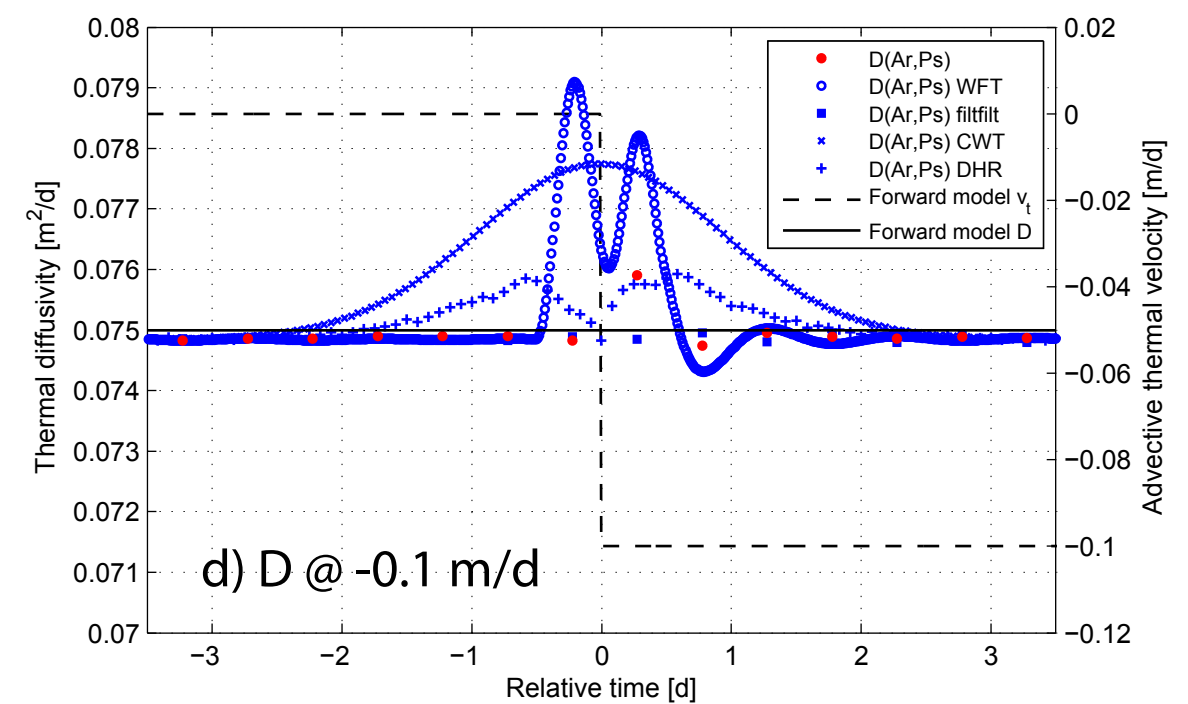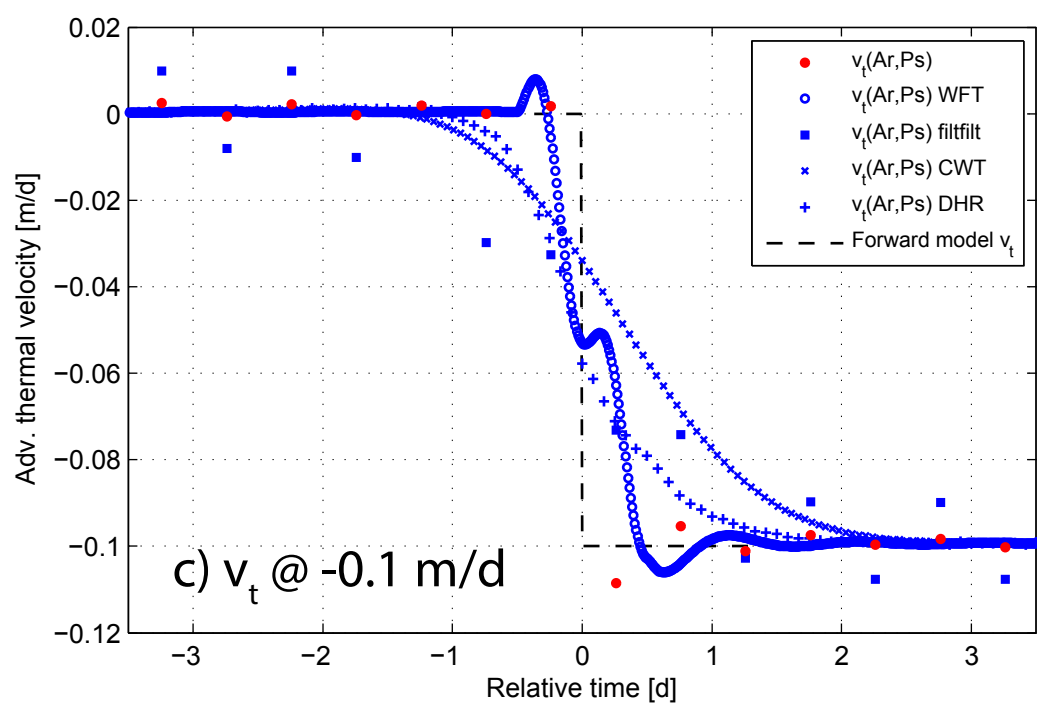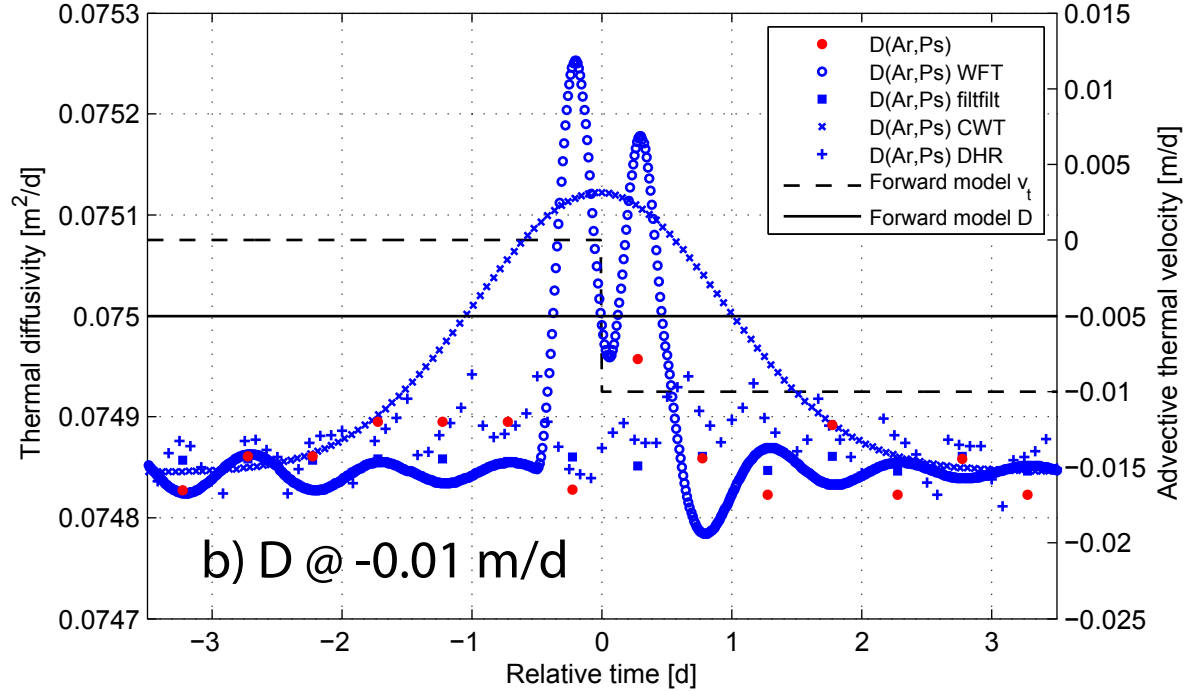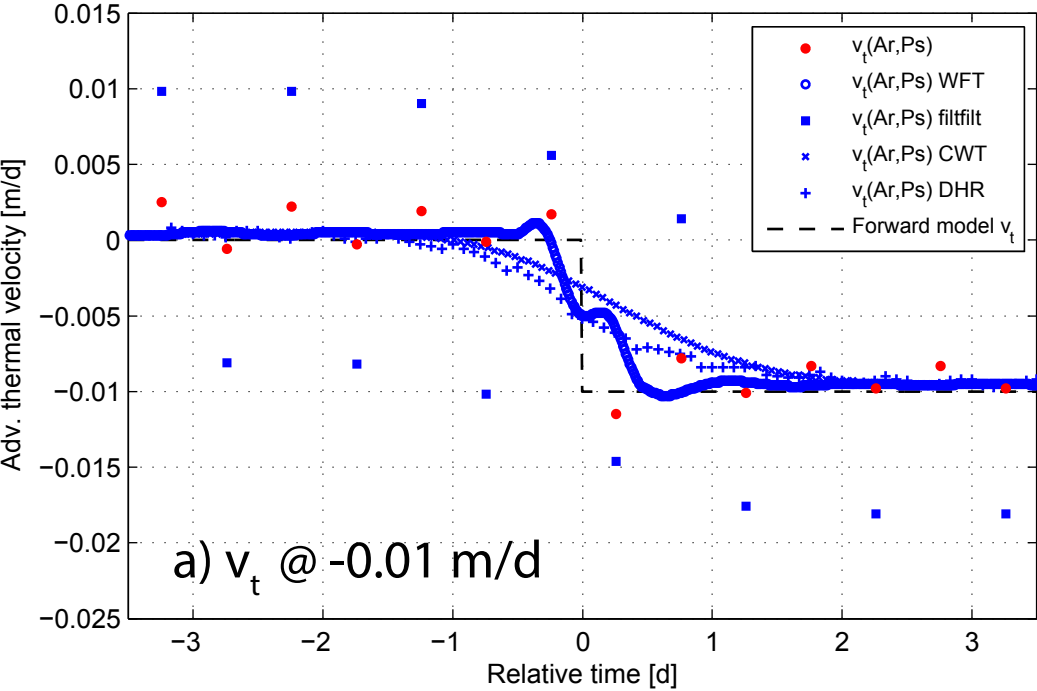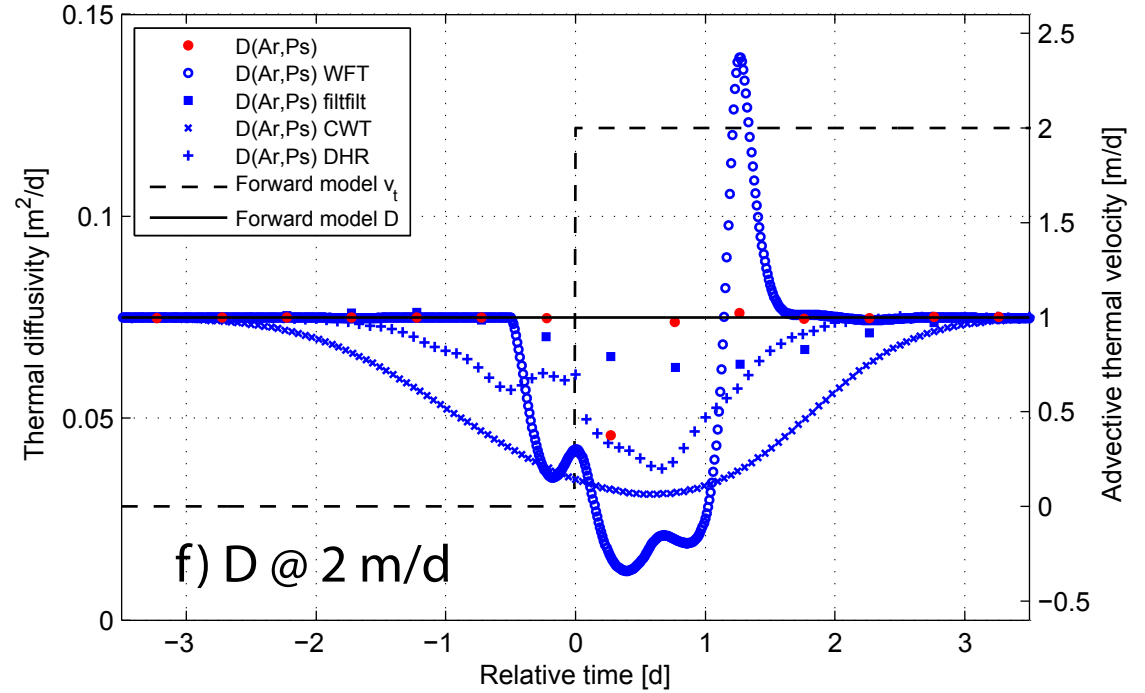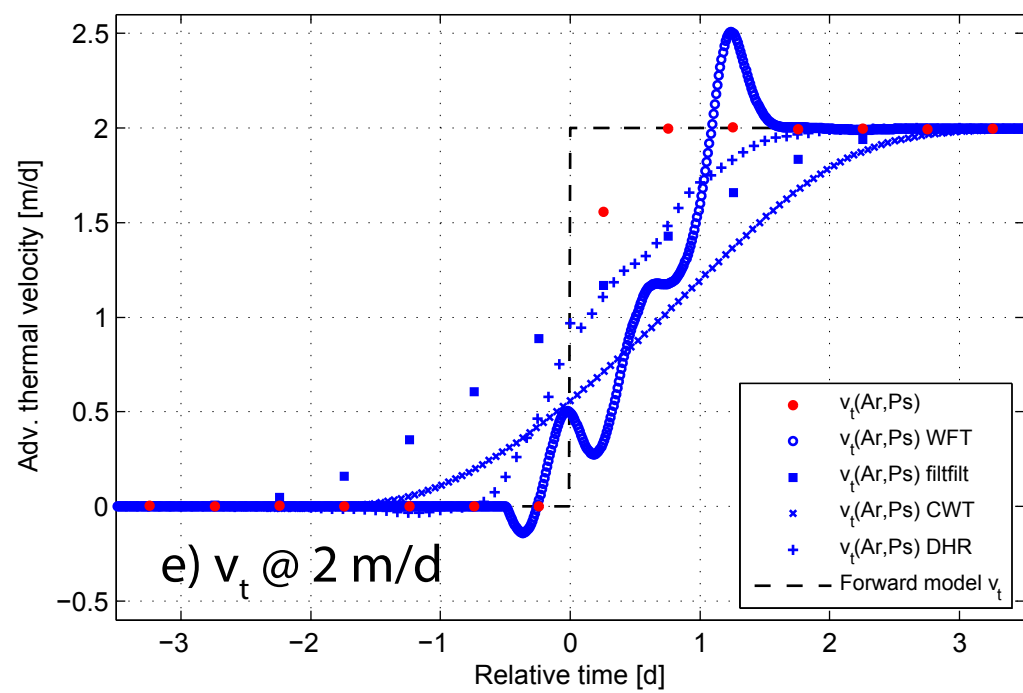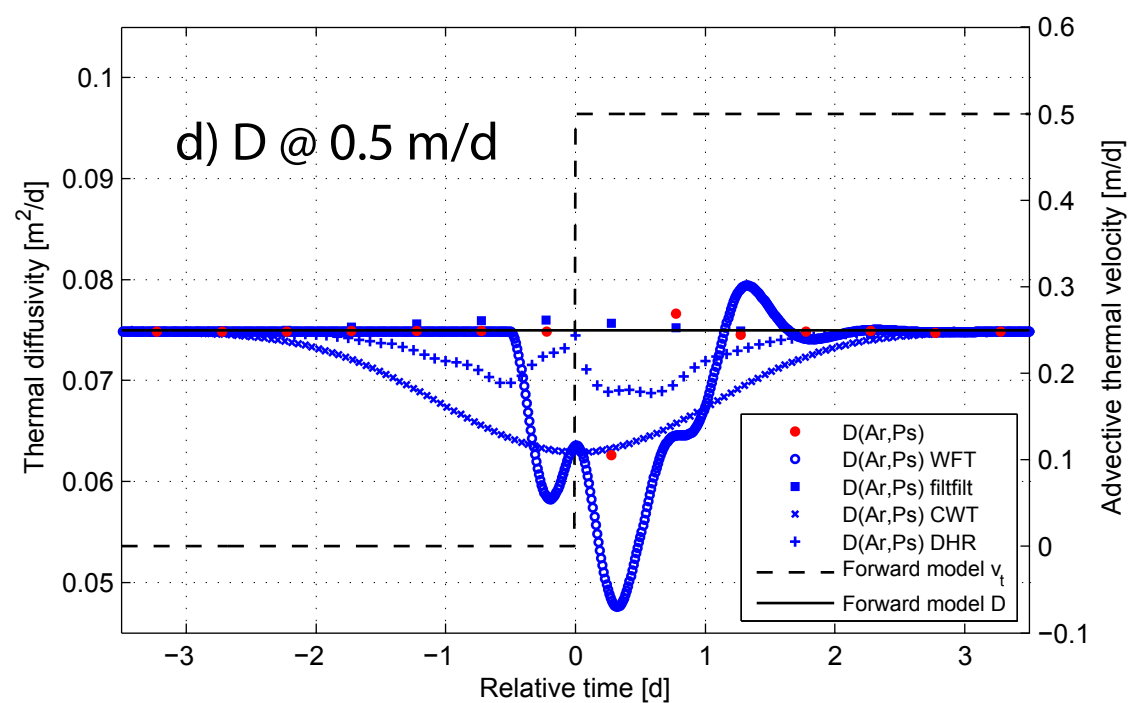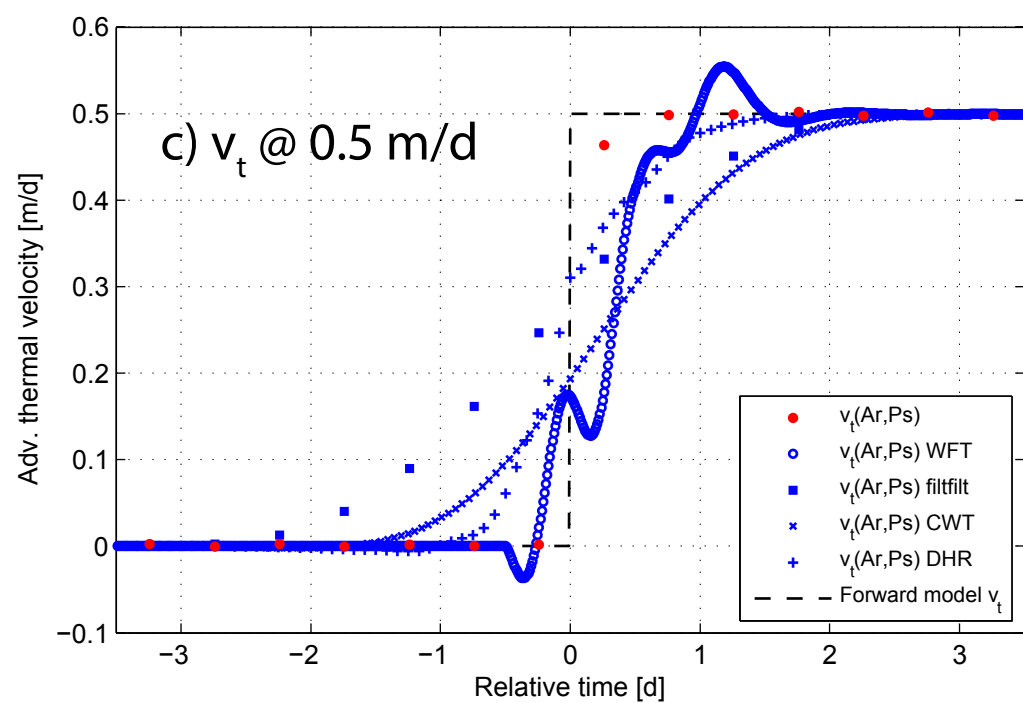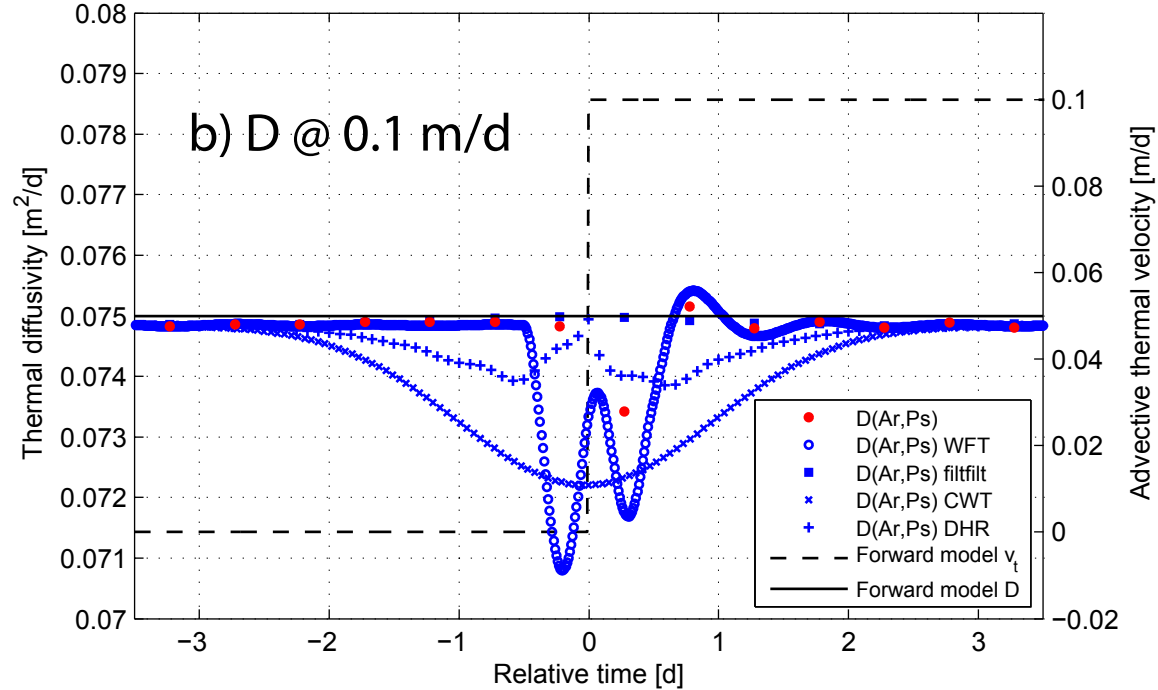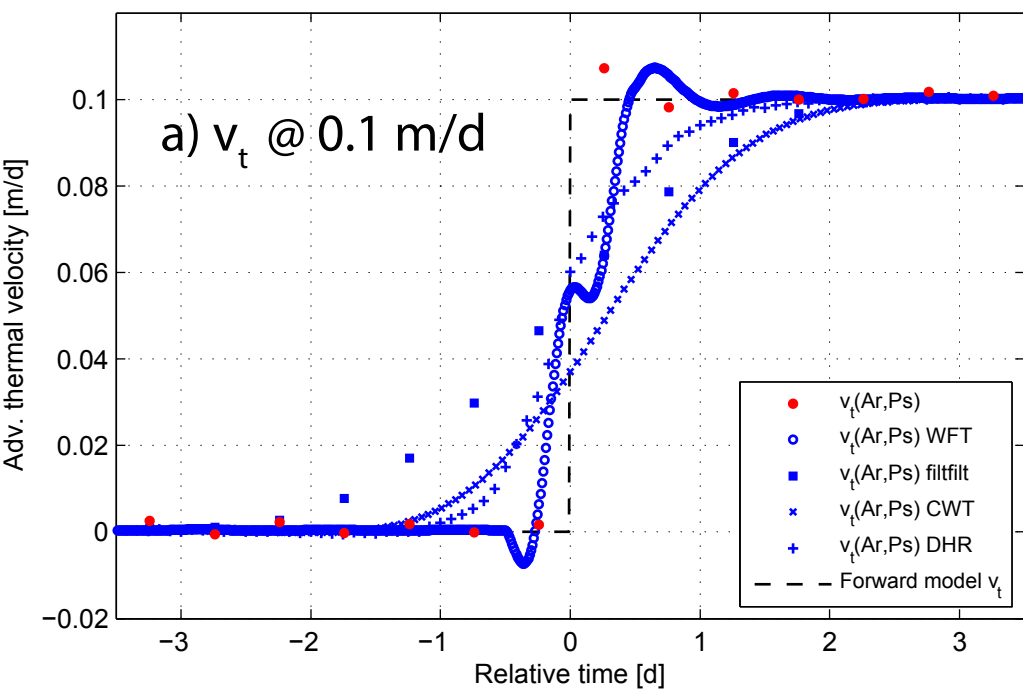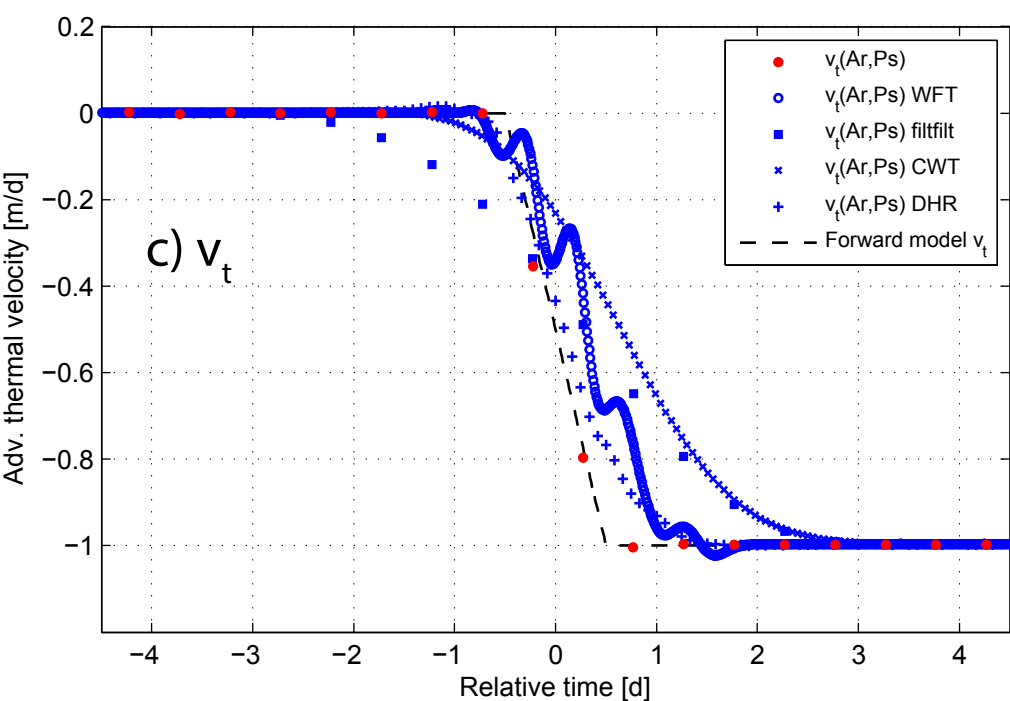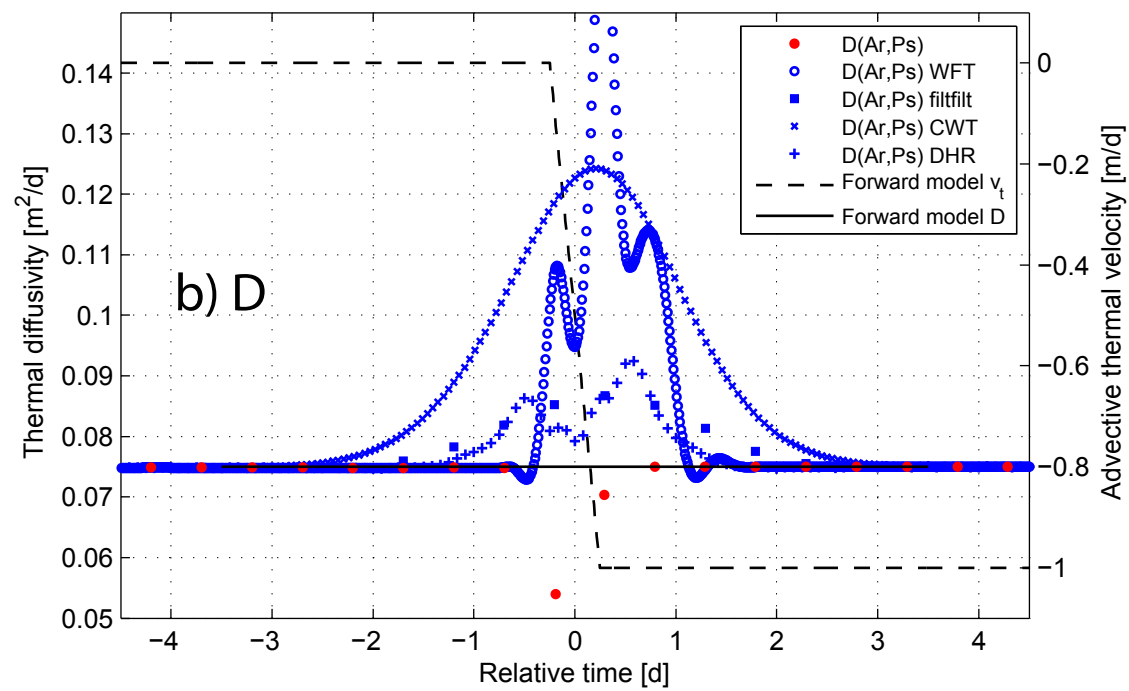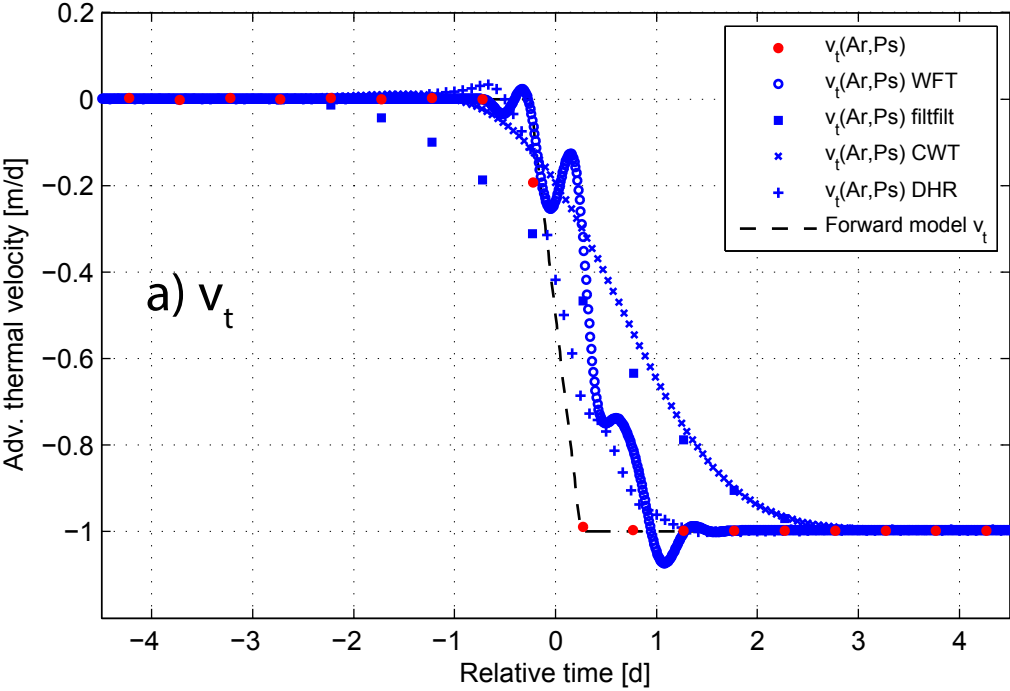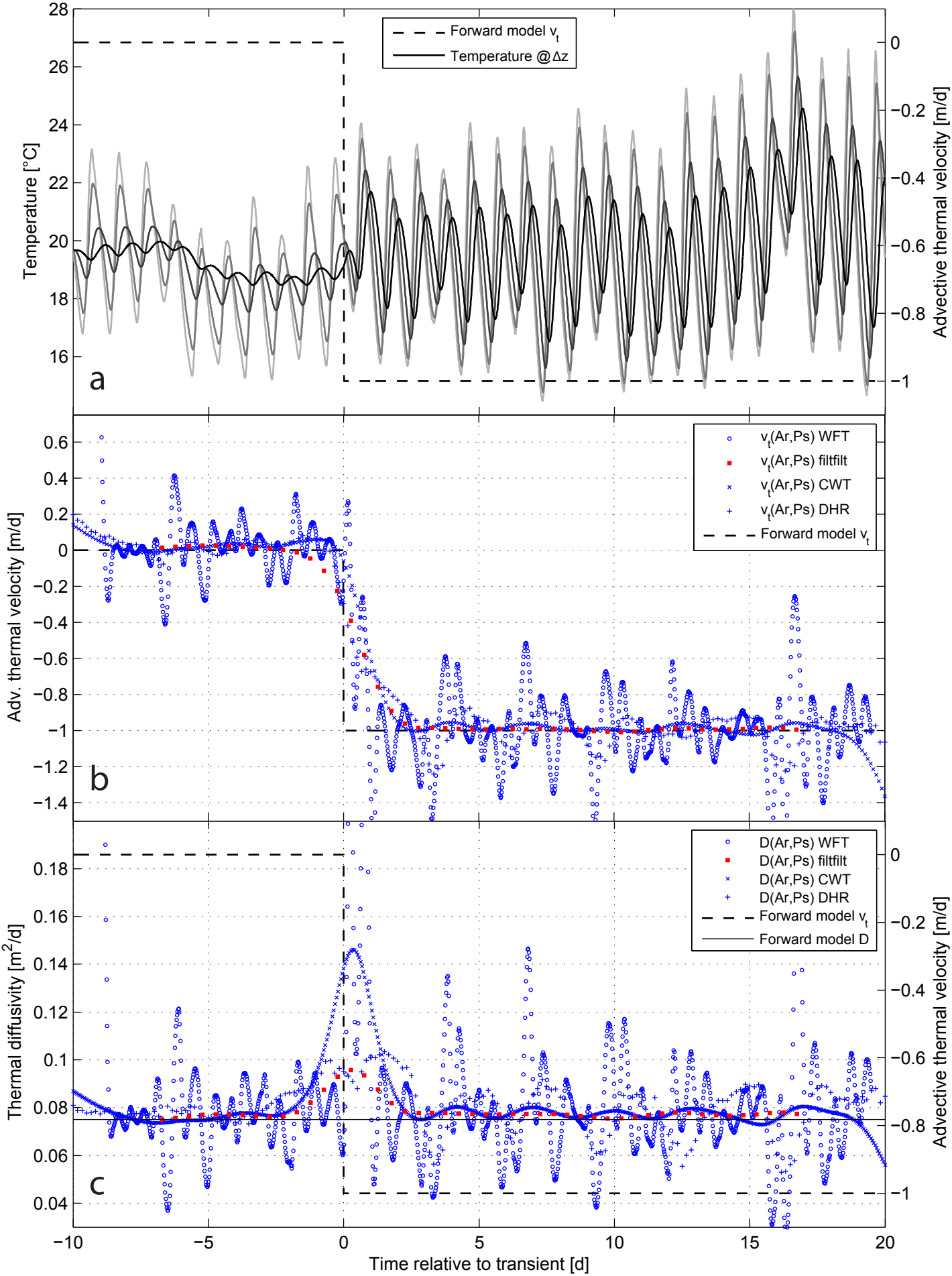
Rate of velocity change dv/dt [L/T^2]	Max. thermal velocity error [m/d]					RMSE [^{o}C]				
	No filter	WFT	filtfilt	CWT	DHR	No filter	WFT	filtfilt	CWT	DHR
-0.25	-0.03	0.12	0.11	0.18	0.06	0.011	0.050	0.055	0.090	0.020
-0.5	-0.05	0.21	0.23	0.36	0.12	0.015	0.069	0.098	0.130	0.030
-1	-0.08	0.40	0.35	0.56	0.23	0.019	0.098	0.134	0.167	0.049
-2	-0.13	0.75	0.53	0.70	0.31	0.031	0.134	0.181	0.193	0.067
-∞	-0.04	0.99	0.50	0.83	0.57	0.011	0.208	0.177	0.247	0.134

1

2 Table 1: Summary of maximum error and root mean square error (RMSE) calculated from modeled and inverted advective thermal velocities
3 using unfiltered and filtered temperature data for the same magnitude velocity transients (0 to -1 m/d) but for different rates of velocity change.
4 The values in this table represent a quantification of the results in Figure 8a, 8c, 8e, 8g and Figure 5a.

Rate of velocity change dv / dt [L/T^2]	Max. thermal diffusivity error [m^2/d]					RMSE [^{o}C]				
	No filter	WFT	filtfilt	CWT	DHR	No filter	WFT	filtfilt	CWT	DHR
-0.25	-0.004	0.014	0.001	0.018	0.003	0.002	0.006	0.001	0.011	0.002
-0.5	-0.008	0.030	0.005	0.032	0.006	0.003	0.010	0.002	0.014	0.002
-1	-0.012	0.063	0.010	0.044	0.013	0.004	0.014	0.004	0.018	0.004
-2	-0.021	0.097	0.012	0.049	0.017	0.005	0.018	0.005	0.020	0.005
-∞	0.000	0.156	0.014	0.056	0.025	0.000	0.031	0.006	0.026	0.008

1

2 Table 2: Summary of maximum error and root mean square error (RMSE) calculated from modeled and inverted thermal diffusivities using
3 unfiltered and filtered temperature data for the same magnitude velocity transients (0 to -1 m/d) but for different rates of velocity change. The
4 values in this table represent a quantification of the results in Figure 8b, 8d, 8f, 8h and Figure 5b.